Superconducting-magnetoresistive sensor: Reaching the femtotesla at 77 K

Myriam Pannetier-Lecoeur

Habilitation à Diriger des Recherches

Présentée par

Myriam Pannetier-Lecoeur

Service de Physique de l'Etat Condensé – CEA Saclay

Superconducting-magnetoresistive sensor: Reaching the femtotesla at 77 K

Soutenue le 28 Janvier 2010 devant le jury composé de :

- Claire Baraduc, SPINTEC-CEA-Grenoble ; France (rapporteur)
- Claude Chappert, Institut d'Electronique Fondamentale, Orsay ; France (rapporteur)
- John Michael David Coey, Physics Department, Trinity College Dublin ; Ireland (examinateur)
- Claude Fermon, SPEC-CEA-Saclay ; France
- Risto Ilmoniemi, BECS, Aalto University Helsinki ; Finland (rapporteur)
- Jérôme Lesueur, ESPCI-UPMC, Paris ; France (examinateur)

Contents

Introduction

My research activities have been first focused on high-T_c superconductivity (PhD and first post-doctoral fellowship). During my PhD thesis, I have studied Abrikosov vortex dynamics in type II superconducting structures through transport measurements. During my post doctoral stay in Amsterdam I had investigated the flux penetration in bulk and thin films superconductors with the aim of magneto-optical imaging.

Since I arrived at the Service de Physique de l'Etat Condensé at CEA Saclay, end of 2001, I have been involved in understanding of transport and noise mechanisms in nanoscale magnetic structures and in spin electronics systems, such as spin valve Giant Magneto-Resistances (GMR) and Tunnel Magneto-Resistances (TMR). Exploring the underlying phenomena, especially in the low frequency noise, led me to develop magnetic field and current sensing devices with improved performances. Part of the sensor development is related to room temperature applications, dedicated to industrial needs (2D compass, voltage monitoring in fuel cells…), magnetic imaging system (non destructive evaluation, magnetic mapping for Earth field sciences) and also for magnetic biochips.

In order to measure extremely weak fields, in particular those produced during the cognitive tasks by neuronal activity, we have proposed and realized femtotesla sensors (or mixed sensors) based on the association of spin electronics and superconductivity, which offer an alternative in thin film technology to the most sensitive existing devices, the low T_c SQUIDs (Superconducting Quantum Interference Devices).

In this report, I present in the first part the state of the art and requirements for magnetic field measurements in the low value range (lower than 1 µT), then I detail the principle, realization and characteristics of the mixed sensors.

Amongst the weakest magnetic signal of interest are those produced by the body, in particular the heart and brain electrical activity, and the resonant signal of nuclei excited through Nuclear Quadrupolar Resonance (NQR) and Nuclear Magnetic Resonance (NMR) experiments. I show in the third part how we succeed in using mixed sensors to detect the magnetic heart signal. Resonant experiments have been also successfully carried to perform solid explosives detection by NQR, and proton NMR, opening way to low-field MRI, as detailed in the fourth part of this report.

Magnetic sensors

Sensing the magnetic field

For more than four thousand years, men have developed instruments to probe one of the most mysterious and fascinating phenomenon, the magnetic field. First by building up compasses to indicate the direction of the Earth field, then later exploiting some properties of materials, like Hall effect or induced current (Ampere law) to measure the strength of the field. From the discovery of electrical current and of the link between current and field in the XIXth century, needs of accurate sensors to measure both field and current had led to many devices. Most of them are still widely used in many applications, from current sensing in cars or electricity meters, to navigation systems in aircraft or spatial probes.

As the magnetic field can exhibit a wide range of amplitudes and frequencies, a large variety of sensors is needed to probe it in the correct range.

Figure 1 illustrates the 15 orders of magnitude in magnetic field one may find in our environment and four kinds of magnetic sensors based on different physical effect that might be used, depending on the strength of the signal.

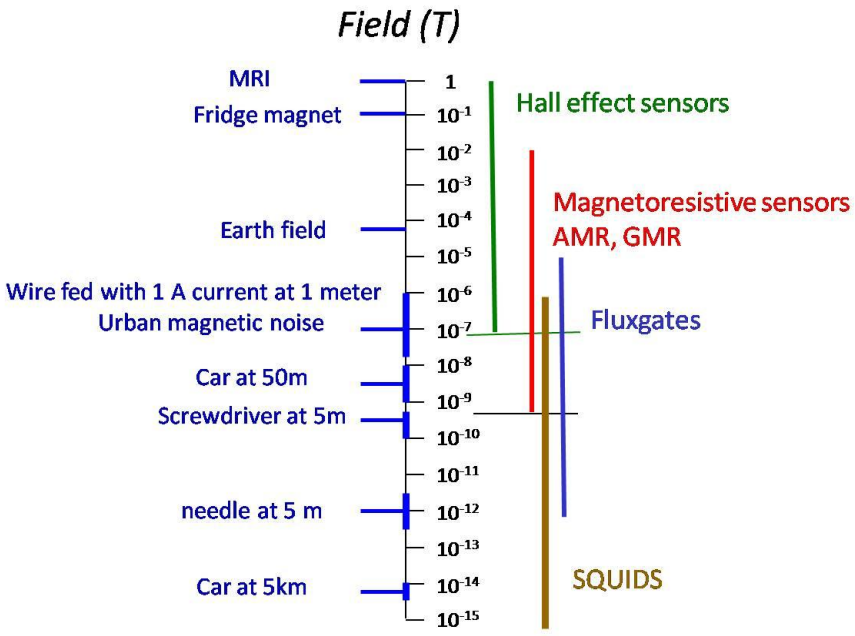

Figure 1 : Scale of quasi-static magnetic field generated in our environment compared to the range of sensitivity of few commonly used magnetic sensors.

One may classify the magnetic sensors by their detectivity, which is their ability to detect a certain level of signal (in tesla) over their intrinsic noise [1] .

Here I will focus on the most sensitive sensors, those addressing signal much lower than the Earth magnetic field, ultimately like those emitted by the electrical currents circulating in the body (heart, neurons, nerves…) whose strength ranges from picoteslas (10^{-12}T) to femtoteslas (10^{-15}T).

Sensitive and highly sensitive magnetometry

A proper sensor will be defined by the signal which is targeted. First characteristic, but not the sole, is the amplitude of this signal in tesla (or A/m). Another very crucial aspect is the source size and its distance. A small sensor may not be appropriate for a distant source. On contrary, a very sensitive sensor integrating the signal over a large surface might not be fitted to a very local source. The environment is also a key parameter for the choice of the sensor. Environmental conditions (noise, temperature range, vibrations…) and dynamics are also important parameters to be taken into account.

Below the microtesla, four technologies can be depicted for field sensing, each of them presenting advantages and drawbacks. The first two technologies (Hall and MR sensors) are sensing the magnetic field, whereas the last three (coils, fluxgates and SQUIDs) are sensing the magnetic flux over a surface. This distinction will be important also in the applications.

Field sensors:

Hall effect sensors

The first technology and oldest known is based on the Hall effect. Discovered by Edwin Herbert Hall in 1879, it is described as the appearance of transverse voltage in a conductor biased with a current and over which a perpendicular field is applied. The motion of charge carrier deflected by the magnetic field is responsible of this voltage which is directly proportional to the applied field (see Figure 2).

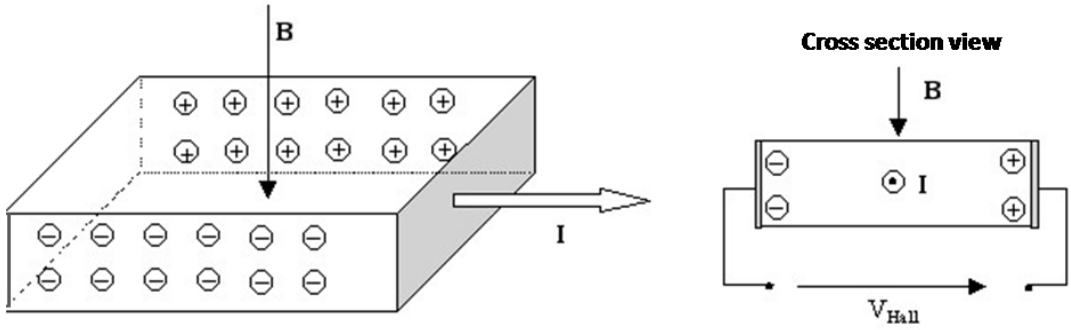

Figure 2 : Hall effect principle.

A Hall effect sensor is a linear absolute sensor and its sensitivity can be below the microtesla. These sensors are rather cheap and can be reduced to micron-sized with the help of semiconducting material and 2D-electron gas (Hall microprobes). They probe the out of plane component of the field.

AMR and GMR sensors

Second technology is using the magnetoresistive effect. First discovered, the anisotropic magnetoresistance is the property of some metals to see their resistance changing in the presence of an applied field (parallel to the plane). This effect is rather small (less than 3% in 1 mT) and requires a certain volume of material to be measured. The AMR sensors are quite cheap to fabricate, with sensitivity in the order of 1 to 100 nT/√Hz. They present a saturation point in the mT range and are not absolute sensors.

Another magnetoresistive effect, the giant magnetoresistive effect, has been discovered experimentally in 1988 by Albert Fert and Peter Grünberg, in thin films stacks of Fe/Cr. The Giant Magnetoresistance is based on the spin polarized transport. This effect will be more detailed in the next part. GMR sensors are not absolute sensors and have also a saturation that may limit their operating range. Their sensitivity is better than Hall effect or AMR sensors, down the 0.5 nT/√Hz at room temperature. They are widely used in hard disk read heads where they detect the magnetic coding of the bits.

Flux sensors:

Coils

From Faraday's law, the voltage in a coil is given by the variation of the magnetic flux:

$$V_i = \frac{d\Phi}{dt}$$

which is the basis of principle of inductive sensors.

The sensitivity of a conventional air coil will directly depend on the surface of the coil and on the magnetic field frequency. Such a sensor operates from kHz to GHz with a detectivity ranging from pT to sub fT. For 1 MHz, the sensitivity of a tuned coil is about 1 fT/√Hz.

Coils are unbeatable flux sensors when size is not a limitation and for high frequency. In particular, they are used for MRI experiment when the signal is probed over large surface and at hundreds of MHz. At low frequency, the signal-to-noise ratio decreases strongly and limits the performances of the coil. Furthermore, miniaturization leads to reduction of performances as well.

Fluxgates

A fluxgate comprises a ferromagnetic core excited by an ac current fed into a winding around the core; the permeability is changing as twice the frequency *f* of the ac current, and in presence of a dc magnetic field, the core flux changes also with 2*f*. Fluxgate sensors are solid state devices measuring static or low frequency fields from 10^{-4} down to 10^{-10} T [1] . As the sensitivity of the fluxgates is proportional to the surface of the magnetic core, they are flux sensors.

Fluxgates can operate at room temperature with sensitivity in the order of few picoteslas, but contrary to the other sensors presented here, they can hardly be made out of thin film

technology to allow integrated devices. They are very useful for far sources detection when size is not a problem.

SQUIDs

Although all these sensors show performances that explain the wideness of their use, they cannot compete so far with the most sensitive magnetometer in the largest range of frequency which is the Superconducting Quantum Interference Device (SQUID). The SQUID is based on the Josephson effect, which appears when two superconducting materials are separated by a very thin insulating layer (Josephson junction) [2] . The phase difference between the two superconductors is generating a constant voltage. If one drives a constant current on the junction, the voltage oscillates at a frequency depending on the bias current and on the superconducting gap. The sensitivity of such an element is already rather good, but is really enhanced when introducing two junctions in a loop, allowing the device to see changes in the magnetic flux of this loop, leading to sensitivity of $10^{-7}\Phi_0$, Φ_0 being the flux quantum, equal to $2.07.10^{-15}$ T.m^2. Sensitivity of SQUIDS is depending of the size of their pick-up loop, typically 1-3 fT/√Hz for a 20x20 mm^2 loop. Best SQUIDs are made out of low T_c materials, typically Niobium, where the junction fabrication is reproducible with a metallic layer oxidized in-situ. High T_c SQUIDS, based on the $YBa_2Cu_3O_{7-\delta}$ (YBCO) cuprate (T_c=92K) have been also realized, but as this material requires epitaxial growth to be superconducting, the fabrication of the junction is more difficult (usually addressed with the aim of bicrystal where the superconductivity of the YBCO is locally destroyed or by ramp edge deposition). High-Tc SQUIDs have sensitivity of the order of 30 fT/√Hz and are difficult to obtain with reproducible properties.

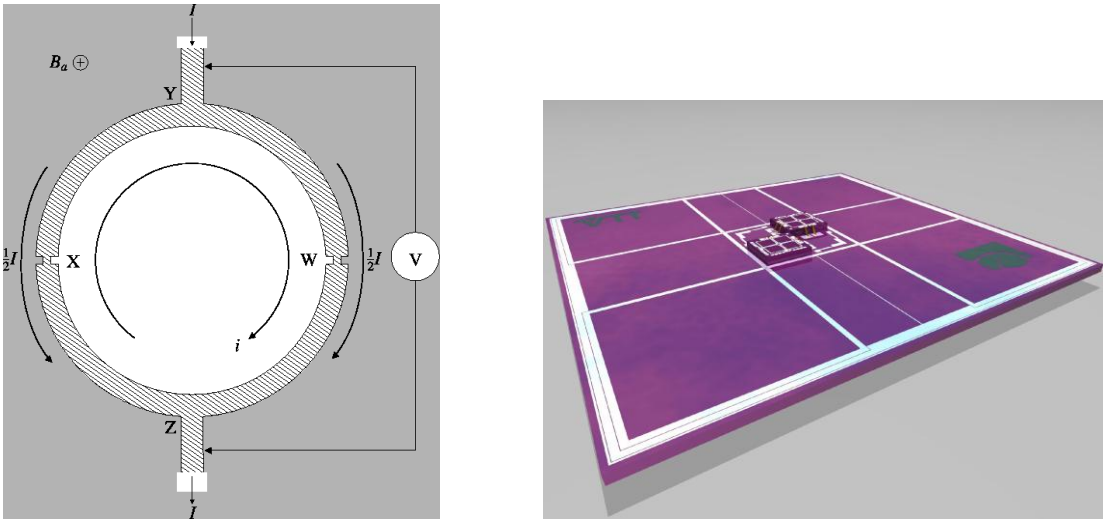

Figure 3 : Left: schematic of the operating SQUID (*from [2])*; Right: schematic view of a low-Tc SQUIDs fabricated at VTT and used in Magneto-encephalography (*Mikko Kiviranta-VTT).*

SQUIDs have been the only type of sensors used for the detection of biomagnetic signals for more than thirty years. In particular, the extremely weak signals generated in the brain during cognitive activities, of the order of few tens of femtoteslas, are only accessible with

low-Tc SQUIDS. Commercial systems of MEG available contain arrays of more than 300 sensors and operate in strongly shielded environment.

The main features of these five types of sensors are given in Table 1.

	Flux/Field	Best sensitivity on 1 Hz band	Frequency range	Advantages	Drawbacks
Hall effect	Field	1 µT	dc-30 kHz	Cheap Linear Absolute	Limited sensitivity
AMR-GMR	Field	0.5 nT	dc-100 MHz	Relatively cheap Sensitive	Dynamics 1/f noise
Coils	Flux	1 fT at 1 MHz, (varies as 1/*f*)	1 kHz-10 GHz	Extremely sensitive Robust	Frequency range, size
Fluxgate	Flux	1 pT	dc-10 kHz	Very sensitive	Large devices
SQUIDs	Flux	1 fT	dc-100 MHz	Extremely sensitive Wide frequency range	Low temperature (4K) Fragile

Table 1: Characteristics of various sensors for magnetic field measurements.

Spin electronics for field and current sensing

Spin electronics can be defined as electronics based on the spin of the electrons and not on the charge of electrons and holes. Technological progress in thin film deposition has permitted the realization and measurements of large effect in the magnetoresistance due to the spin polarization of the material.

Giant magnetoresistance occurs when two magnetic layers separated by a nanometer-thin conductive layer experiences an in-plane field which is acting on the spin of the conduction electron. These electrons can pass from one layer to another more or less easily, depending on the magnetization of the layers. The resistance of the total stack is then varying. In a spin-valve configuration, one of the magnetic layers, called pinned or hard layer, exhibits a magnetization with a high coercivity, which requires fields of several tens of milliteslas at least to rotate. Another layer, called free or soft layer, has a very low coercivity and will see its magnetization rotating very easily in any external applied field.

In detail, the pinned layer generally comprises at least two layers, an antiferromagnetic like PtMn or IrMn coupled to a ferromagnetic layer with a high spin polarization, such as CoFe. The antiferromagnet pins the magnetization of the CoFe by a strong coupling at the interface. The orientation of this layer is realized during the deposition by applying a field in the wanted direction. The free layer is often the association of a CoFe, to a very soft ferromagnet, like NiFe, which rotates extremely easily in the field.

Spin valves are particularly suitable for sensing purpose, since their response in field exhibits a linear variation in the operating field range (see Figure 4).

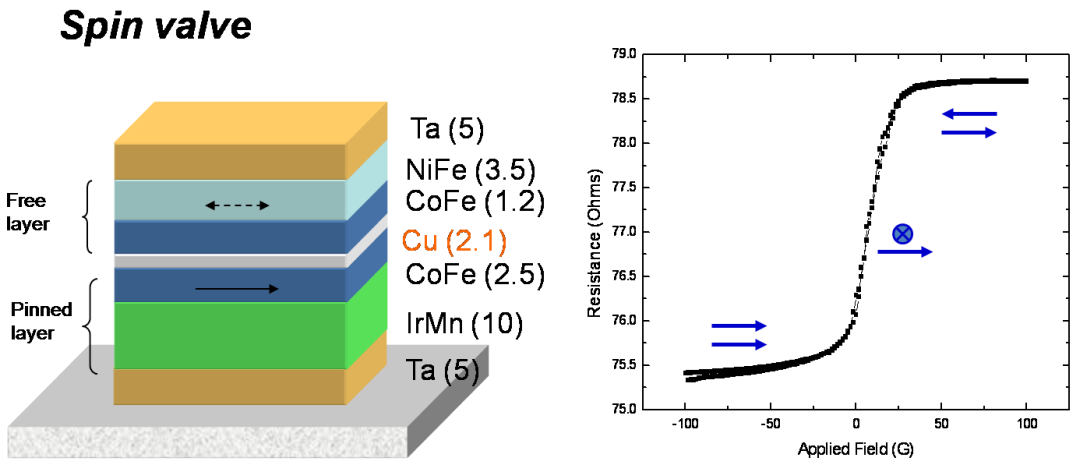

Figure 4 : Left: typical spin valve GMR element. Right: Resistance as a function of the in-plane applied field for a spin valve sensor.

As GMRs are field sensors, their response is not depending on the size, so micron sized elements can be fabricated. Commercial systems are available, allowing field and current measurements with nT/√Hz sensitivity. As the technology of fabrication of these layers are now well mature (due to the huge development for read heads), GMR are good candidates to replace AMR and sometimes Hall sensors in automotive or household goods market.

Due to their small size, these sensors can also be used to field mapping purpose, where a single sensor integrating several elements can be used. Figure 5 shows an example of static field mapping realized in our laboratory for Earth Sciences applications, in particular micrometeorite magnetization mapping.

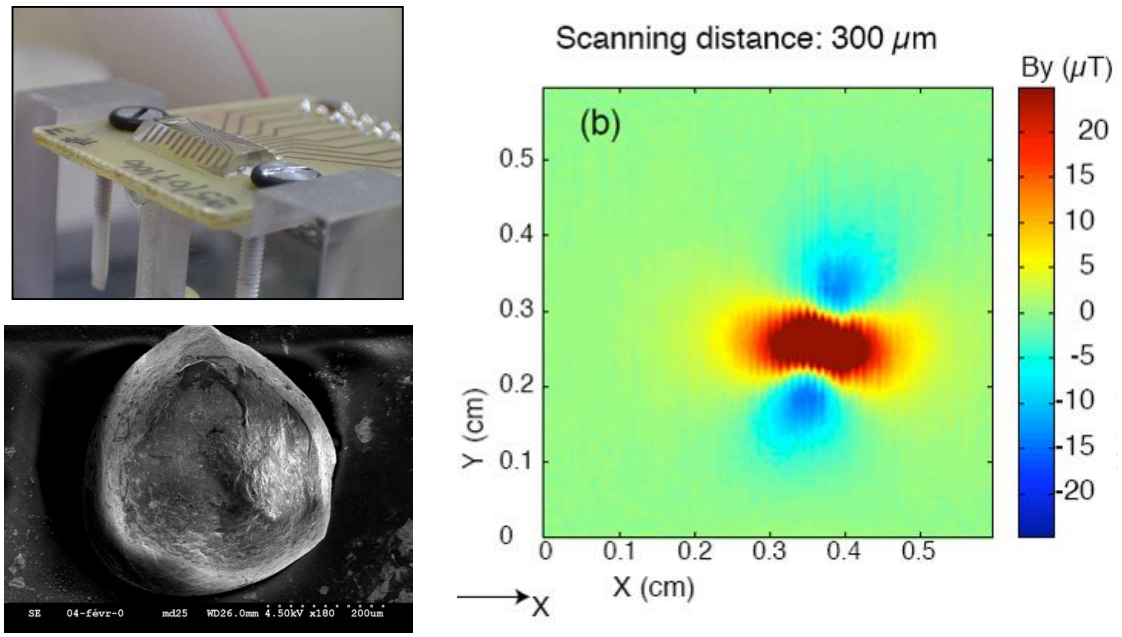

Figure 5 : Left: GMR scanning element for magnetic field mapping. SEM picture of a 450µm meteorite collected in Antarctica, Right: Magnetic mapping of the meteorite magnetic dipole. *Coll. Cerege – Jérôme Gattacceca.*

Proposal for a new type of sensor

Solid state sensors can be classified in two kinds: field sensors and flux sensors. The most sensitive sensors are flux sensors. Nevertheless some field sensors offer already a good level of detectivity. In the problematic of getting a larger choice of possible sensors, one may think of increasing the performances of field sensors by adding to them an element which would enhance locally the field by concentrating the flux over a surface. This has been addressed with flux guides, made out of soft ferromagnet. In a static configuration, the field lines are concentrated to the smaller dimension of the flux guide, with an effective gain of about 30 to 50. This gain has to be put in balance with the increased size of the device. Even though the sensitivity can be increased, a strong limitation arises due to the formation of magnetic domains within the soft material, which may lead to an increase of the magnetic noise, reducing therefore the signal-to-noise ratio.

In even smarter devices, the flux guide is suspended in the vicinity of the field sensor, and oscillates in order to modulate the signal in a range of frequency where the sensor is the most sensitive ([3] [4]).

But the best flux concentrator on a wide range of frequency is offered by a superconducting material shaped in a loop. The flux caught will be related roughly to the surface on this loop. The physical reaction of the superconducting to loop to a perpendicular field is the generation of a supercurrent flowing in the loop to prevent the entrance of the flux in the superconducting area. This supercurrent itself generates self field lines which circle through the hole of the loop (see Figure 6). A field sensor located in the vicinity of these field lines can detect them. In that way, by combining a superconducting flux transformer to a field sensor, we obtain a new type of magnetometer.

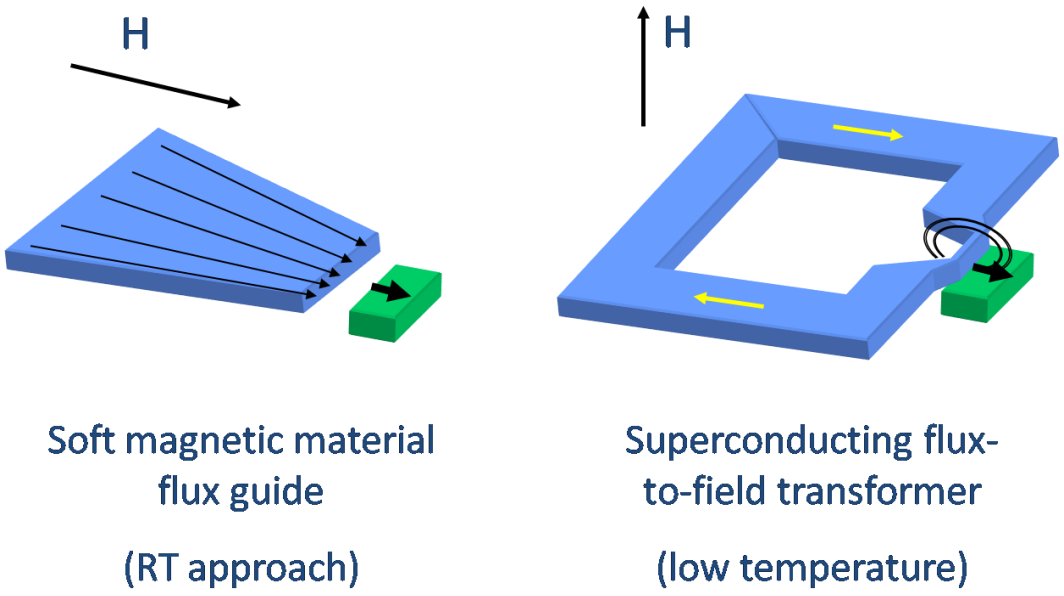

Figure 6 : Flux transformers. Left: soft magnetic flux guide (room temperature approach); Right: superconducting flux transformer. The field sensor element is shown in green.

Mixed sensor: principle, fabrication, characteristics

From the idea of associating a superconducting flux transformer (to catch the flux over a large surface) to a field sensor, it is possible to develop a new device, whose performances should be high enough to counteract the cost of the required cooling at liquid nitrogen or helium temperature.

Two elements for the realization of the sensor can be addressed: the flux transformer and the field sensor. Optimizing both is a key point to the relevance of this device.

Principle

Superconducting flux transformer

First part of the sensor to optimize is the flux transformer. Its role is to catch the flux over the largest surface to transform it locally into a strong field. The strength of the field is linked to the value of the supercurrent I_s running in the loop:

$$\Phi = LI_s \qquad (1)$$

The larger the loop, the larger the supercurrent is. The surface of the loop is limited by the technological field targeted. As a maximum value, we will choose the size of the SQUIDs pickup loop for magneto-encephalography, of the order of 25mm diameter. For other application (NMR or RQN), larger loops can be used.

If the superconducting loop contains a constriction, the supercurrent flowing in the loop will locally exhibits a large density, and therefore strong local self-field lines (see Figure 7).

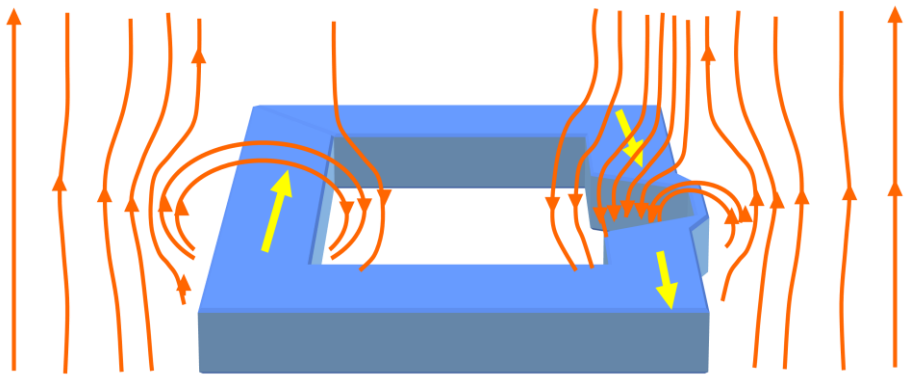

Figure 7: Superconducting flux transformer schematic (here for a square loop). The perpendicular component of the external field will induce a supercurrent (yellow arrows) to flow in the ring to prevent the entrance of the flux. The self-field lines (orange) of the supercurrent are locally stronger at around the constriction, where the current density is the highest.

The supercurrent created in a circular loop by an external applied field is given by

$$I_s = \frac{H_{perp} S}{L} \quad (\mathbf{2})$$

Where *L* is the inductance of the loop and *S* its surface and H_{perp} is the component of the applied field perpendicular to the loop. The inductance for a superconducting loop with a non negligible loop width is given by [5]

$$L = \mu_0 r_L \left\{ ln\left(\frac{8r_L}{w_L}\right) - \alpha \right\} \quad (\mathbf{3})$$

where r_L is the radius and w_L is the width of the loop.

In the case of a thin superconducting ring, the factor α is equal to 2. In the case of a very large superconducting ring, the factor α tends to ¼. Experimentally, we have measured the gain of a mixed sensor, changing the value of w_L while the outer radius is kept constant. The data obtained can be fitted with a linear approximation of α as function of w_L.

$$\alpha = 2 - \frac{7}{4}\frac{w_L}{r_L} \quad (\mathbf{4})$$

If the length of the constriction is not small compared to the size of the loop, one has to add the inductance of the constriction itself and to correct the total loop inductance.

$$I_s = \frac{H_{perp}\pi r_L}{\mu_0\left\{ln\left(\frac{8r_L}{w_L}\right) - 2 + \frac{7w_L}{4r_L}\right\}} \quad (\mathbf{5})$$

For a given size of the loop, the current is maximized for a loop width equal roughly to 0.7 times the radius of the loop.

The field created by the constriction can be calculated from the current given in (5). It depends on the distribution of current in the constriction which is not homogeneous for a superconductor [5] . It varies as the inverse of the width of the constriction as long as the distance between the superconductor and the field sensor is small compared to that width. For a 100 nm distance from the surface of the superconductor and a 150 nm superconductor thickness, 1 A in 5 µm constriction creates a field shown in Figure 8 with a mean value of 102 mT.

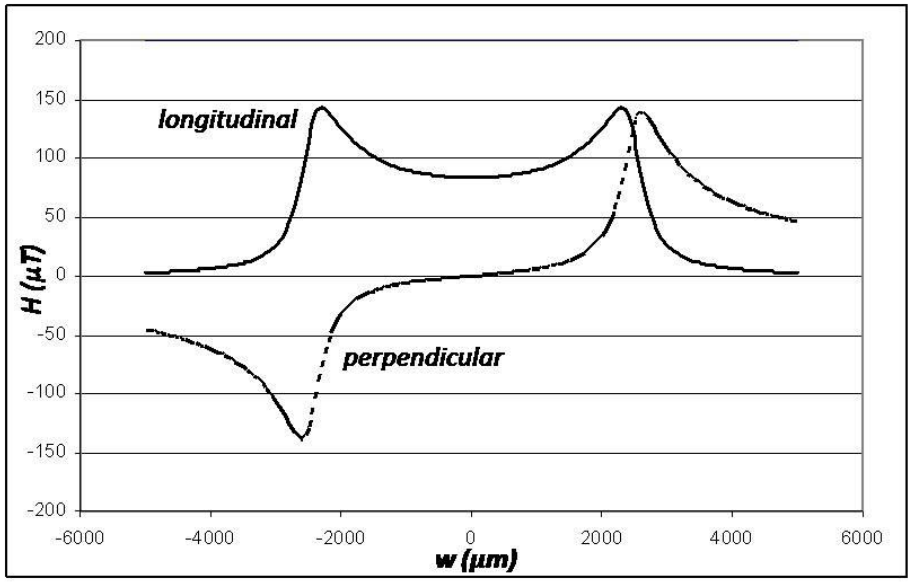

Figure 8 : Perpendicular and longitudinal field component at the location of the constriction for a 1µA current running in the loop.

From eq.(5) and field distribution we can calculate the gain of various flux-field transformers. For further discussion we write:

$$H = gH_{perp} = \frac{g_0}{w} H_{perp} \qquad (6)$$

g being defined as the gain and varies as 1/w. For a 20 mm loop with an optimal width, g is 5000 for 1 µm width constriction (and 1000 for a 5 µm width). Gains experimentally obtained are comparable to the calculated gains.

One experimental measurement of the gain at the constriction location has been obtained by means of magneto-optical imaging, which allows precise mapping of the perpendicular component of the field (for details on the technique see [7]):

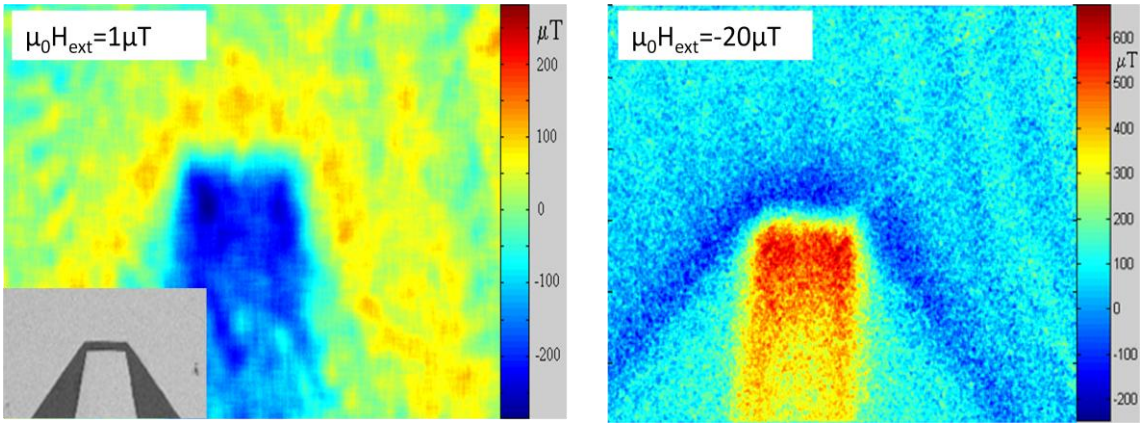

Figure 9 : Magneto-optical imaging of a superconducting constriction in the 3mm-diameter loop of Figure 7, for an applied field of 1 µT (left panel) and -20 µT (right panel). Both images are obtained after a zero field cooling down to 4.2 K. The size of the bridge is 25 µm in length and 7 µm in width. The color scale bar on the right side gives the local field perpendicularly to the film (z-component). Inset: micrograph of the constriction. For a -20µT applied field, the critical current is reached in the constriction leading to limitation of the enhancement factor.

Magnetoresistive element

To sense the locally enhanced magnetic field, one requires a small sensitive field sensor. One option is to measure the z-component of the local field, by placing a Hall sensor in the plane of the loop, closer to the constriction as possible. This approach has been achieved with Hall sensors ([8] [9]) but with rather low sensitivity due to the low sensitivity of Hall sensors and the low efficiency of flux field transformers. The other option, which is the one chosen for mixed sensors, is to measure the in-plane component of the field (perpendicular to the constriction) with a GMR element located on top or below the constriction [10] . The distance between the superconducting loop and the GMR element can be of the order of a hundred nanometers, using thin film technology, i.e. where the field lines are still strong. The width of the GMR element can be the same as the width of the constriction, in the micron range.

The GMR element itself should be nevertheless optimized to increase the sensitivity of the sensor. The main parameters are the GMR stack composition and the sensor design. Signal and noise are key parameters to fully estimate the performances of the mixed sensor.

GMR composition

GMR sensors are built in a spin valve configuration with cross anisotropies: a hard layer (or pinned layer) composed of an antiferromagnetic layer coupled to a ferromagnetic layer is separated from a soft layer (or free layer) by a thin copper layer. The anisotropy of the soft layer is perpendicular to the direction of the magnetization of the hard layer. The typical stack we are using is:
Ta(5nm)/IrMn(20nm)/Cofe(2.5nm)/ Cu(2nm)/CoFe(2.5nm)/NiFe(3.5nm)/Ta(5nm).

One requirement for the GMR stack is to present a rather high magnetoresistance and a low coercivity with no annealing or a short annealing below 230°C. Such condition is necessary for preserving the superconducting properties of YBCO. An annealing at higher temperature induces a fast oxygen loss in YBCO constriction leading to decrease of the critical temperature. A 270°C annealing destroys the superconducting transition of a 5 µm width YBCO constriction.

As mixed sensors operate at 77 K or 4 K, it is necessary to optimize properties at low temperature. For example, ultrathin free layer gives a very high sensitivity at room temperature but it is completely blocked at low temperature. The magnetoresistance (MR) ratio obtained for our GMR stack is about 6% at room temperature and increases to 15% at low temperature. This increase is due to the reduction of spin diffusion in Cu at low temperature and to an increase of the spin polarization at the interfaces. In practice, the highest MR ratio is obtained between 60 and 80 K. At lower temperature, a small decrease is observed because the global resistance is decreasing with temperature and there is no more gain in spin polarization and spin diffusion lengths between 80 K and 4 K.

GMR sensor design

All our GMR sensors have a yoke shape (see Figure 10) which has the advantage to be compatible with the loop shape and presents a very low magnetic noise [11] . Furthermore, instead of using a single GMR element, a bridge configuration might be used, offering several advantages: compensating the drift in resistance of the GMR elements, (due to small temperature variation) and generating an output signal with is only due to the change in magnetic field, avoiding the offset compensation necessary in the case of a single element.

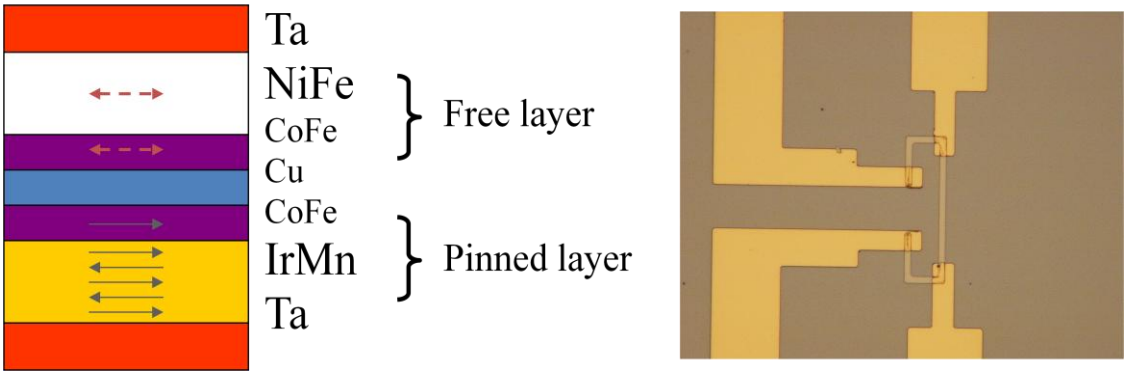

Figure 10 : Left: typical GMR stack (thicknesses are not at scale); Right: micrograph of a yoke shape GMR element with its metallic contacts (for four point measurement).

GMR signal

The output voltage of a GMR sensor in cross anisotropy configuration is simply

$$V = \left(R_0 + \frac{dR}{dH}H\right).I \qquad (7)$$

for small applied planar magnetic fields where I is the injected and R_0 is the resistance is absence of external field.

$\frac{dR}{dH}$ is proportional to R and depends on the inverse of the shape anisotropy of the free layer (created by the dipolar field interactions). Typical thickness of the free layer is 3-8nm. Then the anisotropy is mainly given by the width of the sensor as the length is large compare to it. For 5 µm width GMR and 6 nm-thick free layer, the anisotropy field is about 1 mT. For small widths, the anisotropy is inversely proportional to it. We can then write:

$$\frac{dR}{dH} = \beta(T).R_0.w \qquad (8)$$

where w is the width of the sensor and $\beta(T)$ a coefficient which depends on the exact material composition. At room temperature, we have a typical slope of 2%/mT for low temperature annealed stacks and 5%/mT at low temperature for a 5 µm width and 3.5 nm thick free layer. This gives $\beta(300) = 4.10^3 m^{-1}mT^{-1}$ and $\beta(T) = 10^4 m^{-1}mT^{-1}$ for T<80K.

The resistance R_0 itself varies as the inverse of the width and as the length so we can write:

$$R_0 = r(T)\frac{l}{w} \qquad (9)$$

where *r* is the resistance of a square GMR element. Values of *r* between 12 and 25 Ohms are usual. Generally *r* decreases of about 20% between RT and 4K. For the evaluation of noise, we will take *r*=20 Ω.

If we use a bridge configuration the output voltage of the bridge can then be written as:

$$V_{out} = \beta(T)H.r(T)l.I \quad (\mathbf{10})$$

where *I* is the injected current on the bridge. The limit of the applied voltage is given by the heating of the sensors. At low temperature, a maximal current of 15 mA can be applied on each GMR sensor for a 5 µm width but a value of max 10 mA should be preferred.

GMR thermal and 1/f noise

GMR sensors present two types of voltage noise: the thermal noise which is directly related to its resistance *R,* which can be written as

$$S_{Therm}^{1/2} = \sqrt{4kTR_0} = \sqrt{\frac{4kTr(T)l}{w}} \quad (\mathbf{11})$$

and a 1/f noise (low frequency noise) which is usually written as

$$S_{1/f}^{1/2} = \sqrt{\frac{\gamma_H}{N_c f}} RI \quad (\mathbf{12})$$

where N_c is the number of carriers of the system and *f* the frequency.

This noise comes from low frequency resistance fluctuations. γ_H is a phenomenological constant called Hooge constant [14] . The 1/f noise is proportional to the current and varies as the inverse of the square root of the volume of the whole GMR.

In order to highlight this volume effect, the 1/f noise can be written as

$$S_{1/f}^{1/2} = \alpha\sqrt{\frac{1}{lwf}} RI = \alpha\sqrt{\frac{l}{w^3 f}} r(T)I \quad (\mathbf{13})$$

GMR SNR optimization

The Signal to Noise Ratio (SNR) of the bridge is given by:

$$SN_{Therm} = \beta(T)H\sqrt{\frac{w.r(T).l}{4kT}}.I \quad (\mathbf{14})$$

in the thermal noise regime and by:

$$SN_{1/f} = \frac{\beta(T)H}{\alpha}\sqrt{lw^3 f} \quad (\mathbf{15})$$

in the 1/f noise regime.

In all cases, we have interest to increase the length of the sensor and its resistivity. In the case of the *1/f* regime, increasing the width of the sensor will be important as well.

We see that the 1/f regime SNR is independent on the applied current; therefore decreasing the applied current is preferable. For the thermal noise limited SNR, if the limitation is given by the local power dissipated, equation (10) should be rewritten by introducing $P_m = \frac{r(T)}{w} I^2 l$ which is the power dissipated by unit length. Then eq. 14 can be rewritten:

$$V_{out} = \beta(T) H \sqrt{P_m r(T) l w} \quad \textbf{(16)}$$

Mixed sensor noise evaluation

If we combine (14) and (15) with (16) we obtain the Signal to Noise Ratio (SNR) of the mixed sensor:

$$SN_{Therm} = \beta(T) H_{perp} g_0 \sqrt{\frac{P_m}{4kT}} \quad \textbf{(17)}$$

in the thermal noise regime and:

$$SN_{1/f} = \frac{\beta(T) H_{perp}}{\alpha} g_0 \sqrt{lwf} \quad \textbf{(18)}$$

in the 1/f noise regime.

We see that optimization leads to increase the length and maintain a rather large width for the constriction. However this conclusion is based on the assumption that the anisotropy of the GMR sensor varies as the inverse of the width constriction and hence counterparts the gain of the flux field transformer. There are several attempts at present to use synthetic free layers to reduce the net moment and so this dipolar effect. If these approaches are successful, the calculations given here should be corrected.

Now we can evaluate SN_{Therm} and $SN_{1/f}$ for a realistic sensor. Length is 400 µm (to allow a kOhm range resistance), width 5 µm, resistance 1.6 kOhm, flux-field gain 1000, sensitivity of the GMR 5%/mT.

In the thermal noise regime, SNR is equal to 1 for a field of 30 fT at 67 K and in the 1/f regime for 1 mA and 7 fT at 4 K.

With a 10 mA applied current on the bridge (16 V), the equivalent magnetic noise is 3 fT/√Hz at 67 K and 0.7 fT/√Hz at 4 K. The voltage noise on the bridge is 2.43 nV/√Hz at 67 K and 0.6 nV/√Hz at 4 K. Taking into account the noise of the preamplifier (INA103 preamplifier with 3.2 nV/√Hz voltage+current noise at 300 K), the total magnetic noise is 5 fT/√Hz at 67 K and 3.2 fT/√Hz at 4 K in the thermal regime.

The 1/f noise corner is for 10 mA injected at 10 kHz at 67 K and 1 kHz at 4 K. These corner values lead to a level of noise at 1 Hz of 300 fT/√Hz at 67 K and 21 fT/√Hz at 4 K.

Fabrication

One of the main advantages of mixed sensor is that it is based on thin film technology, and can be produced on various size wafers. Conventional photolithography techniques can be used. Two types of mixed sensors can be fabricated, based on low-T_c or high-T_c superconductor.

I will detail in this section the fabrication of Nb-based and YBCO-based sensors that have been developed in our laboratory. Other techniques might be used as well to fabricate the sensors, depending on the available facilities.

Low-T_c mixed sensor:

Fabrication of low-T_c mixed sensor starts with the realization of GMR sensing elements with their contact pads. Then an insulating layer is deposited over the surface and the superconducting loop made of Niobium is deposited by a lift off technique. The steps used for fabrication are detailed in Figure 11.

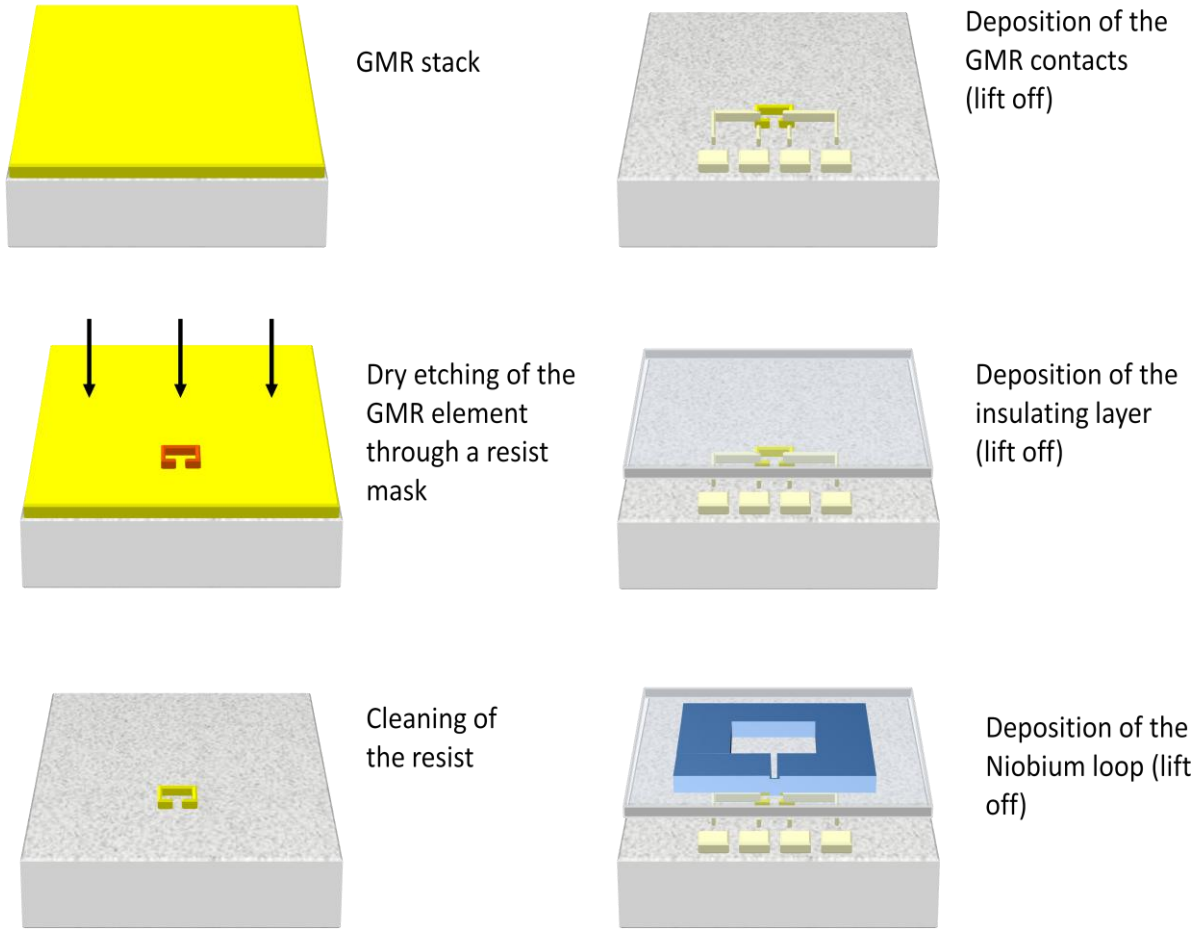

Figure 11: Fabrication steps of a low-T_c mixed sensor (top to bottom, left to right), starting from the GMR stack on the substrate.

High-T_c mixed sensor:

The use of high-T_c superconducting loop allows operating the sensor at liquid nitrogen temperature. As high-T_c thin film requires epitaxial growth conditions on a dedicated substrate and with a high temperature (>600°C) step, it is necessary to fabricate the sensor from the YBCO film. First step is to deposit a thin and flat insulating layer on the YBCO plain film, then to deposit the GMR stack. Quality of the insulating layer is important: it has to be dense (no holes which would shortcut the structure through the superconductor) and flat (roughness would lead to mismatches between the different layers of the GMR stack, reducing strongly the magnetoresistive effect). When these conditions are fulfilled, the patterning process can be applied, schematically described in Figure 12.

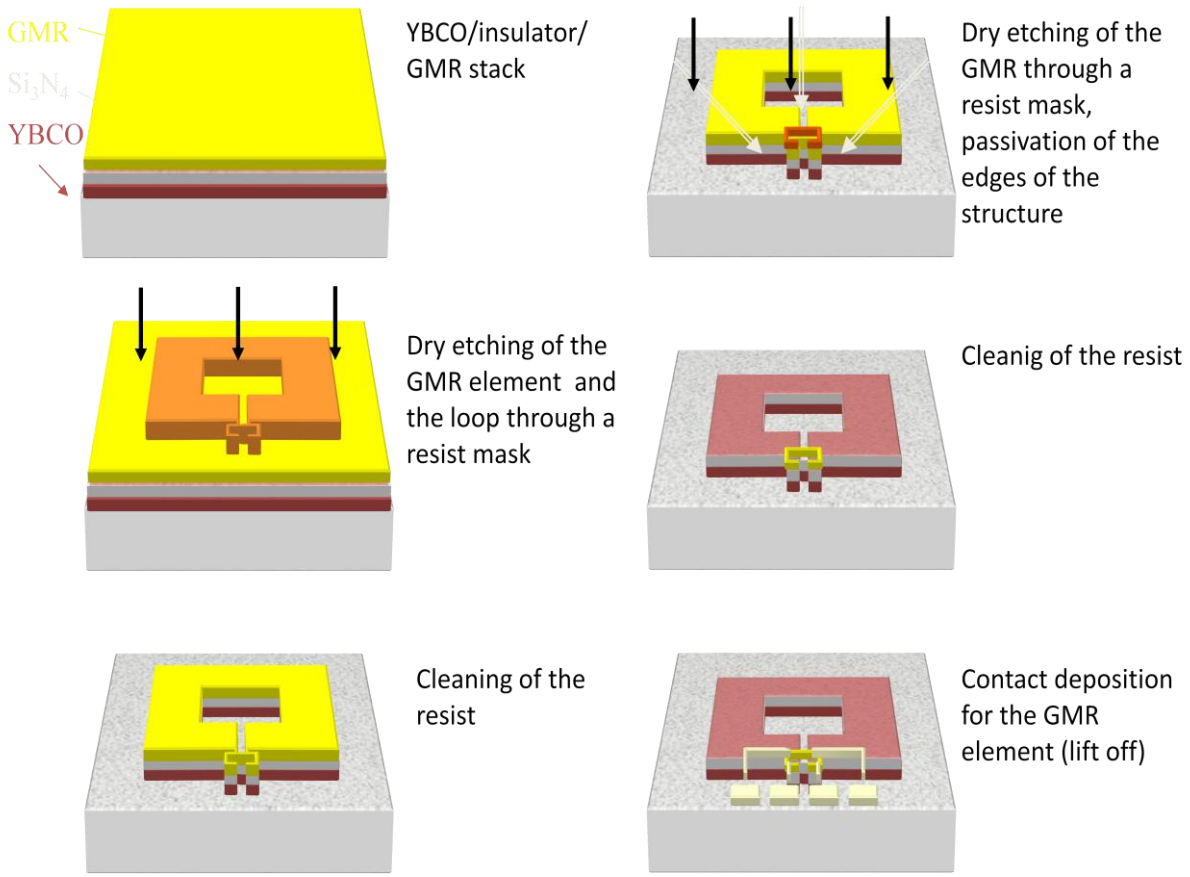

Figure 12: Fabrication steps of a high-T_c mixed sensor (top to bottom, left to right), starting from the GMR stack deposited on the YBCO film (an insulating layer in between the two).

Another way to proceed is to process the YBCO loop first, then deposit the insulating layer and the GMR stack, which can be processed as usual. This method has been applied successfully by Sensitec [12] to process YBCO-mixed sensor on 5" sapphire-substrate (see Figure 13).

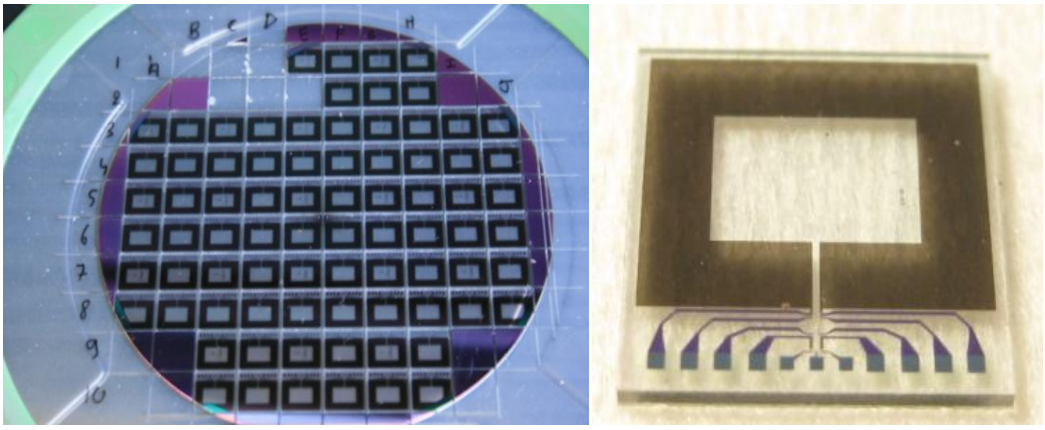

Figure 13 : Left : Photograph of a 5" sapphire wafer processed by Sensitec GmbH [12] to produce YBCO-based mixed sensor. The YBCO layer has been deposited by Theva GmbH [13] . Right: Photograph of one device.

Characteristics

The realized mixed sensors can be characterized through two features: the effective gain of the sensor (*g*) and the noise of the device, which is given by the noise spectrum density of the GMR element. Knowing these two data, we can compare the gain to the calculated value, extract the signal-to-noise ratio as a function of frequency and know the detectivity of the sensor.

Measuring the gain of the sensor

The gain of the sensor can be easily estimated from the comparison of the slope of the GMR element response above T_c in an in-plane field and below T_c in an out-of-plane field.

During the experiment, the GMR response is recorded by sweeping a homogeneous magnetic field up and down in the direction of the pinned layer of the GMR at different temperatures. Below T_c, the same experiment is carried out but with a field applied perpendicularly to the plane of the loop. The GMR element being insensitive to the z-component (out of plane) of the field, the variation of resistance is only due to the self-field generated by the superconducting screening current. This property can be also used to determine the T_c of the constriction, the response getting weaker when approaching T_c and zero at and above T_c.

Both responses (above and below T_c) are shown in Figure 14.

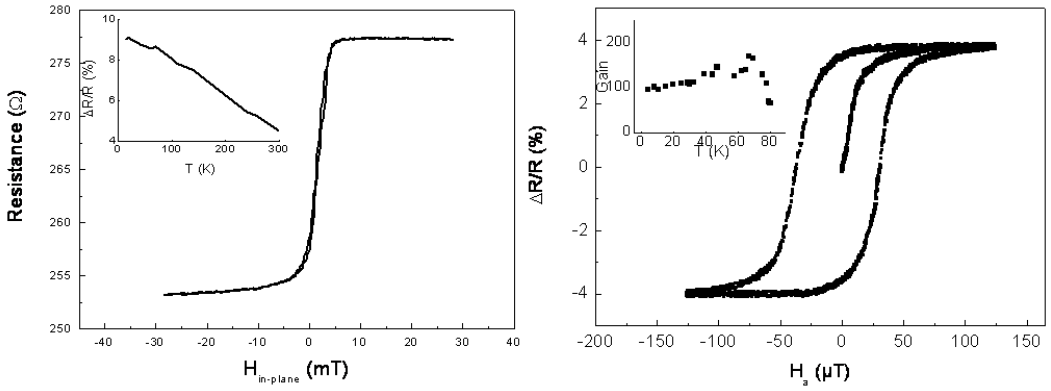

Figure 14: Resistance variation of the GMR element for an in-plane field (left) above T_c and an out-of-plane field (right) below T_c. Note the difference in the magnetic field scale. Insets: Left: $\Delta R/R$ ratio as a function of temperature; Right: variation of the gain *g* as a function of temperature.

On the operating mixed sensor, a saturation of the magnetoresistance ratio occurs usually before the maximum is reached. This is due to the fact that the critical current is reached in the constriction, and therefore, the induced field does not increase anymore. The effect explains also why at higher field, when sweeping back the field, the MR ratio decreases; according to the Bean model [15] , as soon as the field is reversed, the supercurrent starts decreasing in the superconductor.

The field at which the critical current is reached in the constriction depends on the size of the loop (the larger, the sooner), of the size of the constriction (the smaller, the sooner), of the temperature (the cycle is getting smaller and smaller when approaching T_c) and of the quality of the material.

The gain can be calculated simply by the ratio of the two slopes, and compared to the calculated gain. As can be seen in Table 2, a very good agreement is obtained on various sensors.

Samples	*l* (mm)	Constriction width *w* (μm)	Calculated gain g_{calc}	Measured gain g_{meas}
Nb-100	7	7	131	108
Nb-500	25	6	516	500
YbaCuO	3	6	170	160
YbaCuO	18	5	620	600
YbaCuO	20	3	1100	1060

Table 2: Calculated and measured gains of various mixed sensors.

Measuring the noise of the sensor

As the superconducting loop remains in the Meissner state, the main noise source that we expect on the sensor is the noise of the GMR element. The total noise of the sensor can be estimated by measuring the GMR element noise spectrum at low temperature and divide it by the gain *g*.

The noise spectrum is measured either on the output voltage of a single GMR, either on the output on the GMR bridge or half bridge (in the case of Wheatstone bridge configuration).In the case of a single GMR, the output voltage is balanced from an adjustable equivalent resistance. The differential voltage is sent to a low noise amplifier (INA 103), which allows an amplification of 500 with an additional noise of 1.2 nV/√Hz in the thermal noise. After this first level of amplification, the signal is sent to a second filter-amplifier level (Stanford Research 560), allowing high and low pass filtering, and additional amplification. For low frequency noise measurements, a low pass filter in the 10 kHz range is usually chosen to avoid anti-aliasing of higher frequencies noise. In noise spectrum measurements, all additional sources of noise should be reduced or eliminated. In particular, voltage supply noise can be avoided by feeding the sensor current on battery, as well as the amplification chain. Only the acquisition card is plugged on main power. Use of low temperature electronics (at the first stage of amplification) could reduce the total noise to 0.15 nV/√Hz.

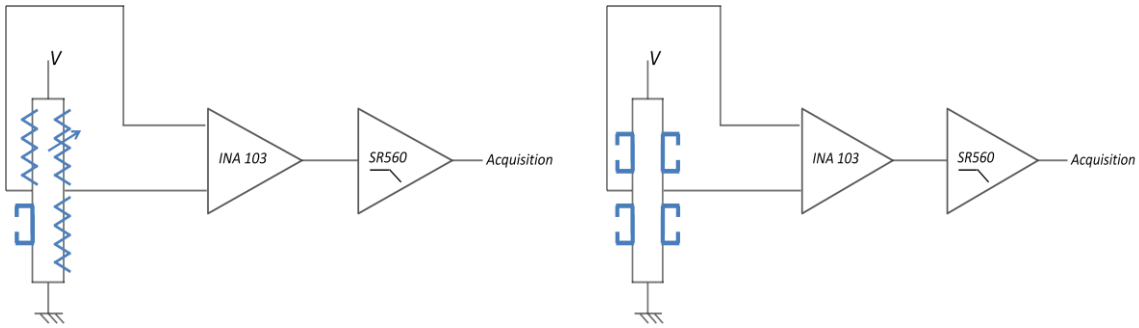

Figure 15: Left: Noise measurement set-up for a single GMR element. Three equivalent resistances are connected, one being adjustable to balance the bridge. Right: Noise measurement setup for a full bridge GMR configuration. The preamplifier (INA 103) has a gain of 500 and the SR560 is set to the maximum gain (up to 1000). A low pass filtering is applied at around 10 kHz to avoid anti-aliasing of higher frequency noise.

Examples of noise spectra and field sensitivities are given in Figure 16.

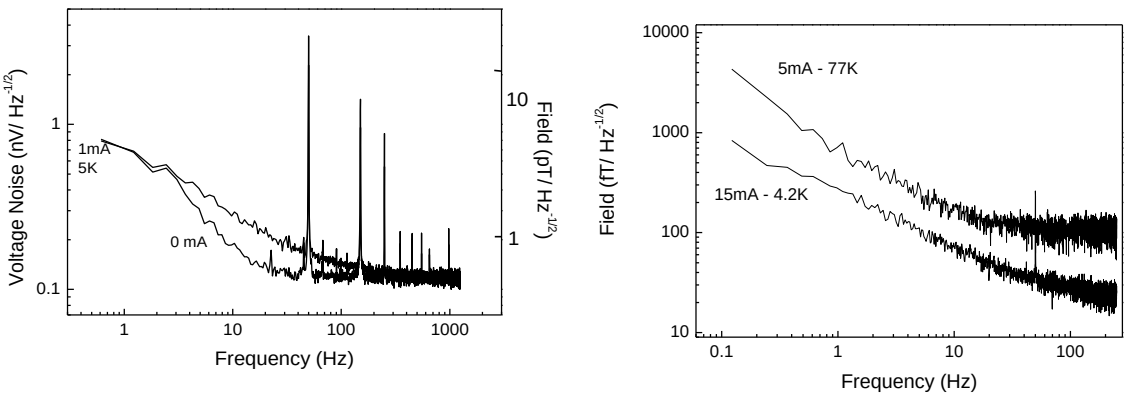

Figure 16: Left: Voltage noise at 4 K for a Nb-based mixed sensor with a 0 mA and a 5 mA sensing current. Right: Field detectivity calculated from the voltage noise spectrum of a YBCO sensor at 4 K (sensing current 15 mA) and 77 K (sensing current 5 mA).

From these spectra, one may observe few characteristics of the noise of the sensors:

First is the importance of the sensing current through the GMR; the higher the sensing current, the better signal-to-noise ratio the sensor will exhibit (in the thermal noise). Limitations in the maximum value of the sensing current are given by the GMR element itself and the operated temperature (currents as high as 15 mA can be used at 4 K or 77 K without destroying the GMR), second limitation being given by the material used for the superconducting loop. For Niobium, the maximum current in the GMR will only be of 1-2 mA, since higher current will bring a local heating of the Niobium constriction and lead to transition to the normal state. This effect is much weaker in the YBCO, which is operated far from its critical temperature.

Secondly, at low frequency, the noise spectra are dominated by the 1/f noise, on which a change in the GMR sensing current will not operate (except to change the 1/f knee frequency value). This noise is strongly dominant below 100-1 kHz and reduces the sensitivity of the sensor in this range. Techniques to reduce this noise are detailed in the next chapter.

A real measurement of the noise of the sensor can be performed in a magnetically shielding room (MSR). This has been realized in the MSR of Neurospin which contains three aluminium/permalloy shields, and exhibits a residual white noise of the order of few pT (to be compared to few nT in our lab). Recorded data are shown in Figure 17, together with a calibrated 5 pT test signal produced with a small dipolar coil at 30 Hz.

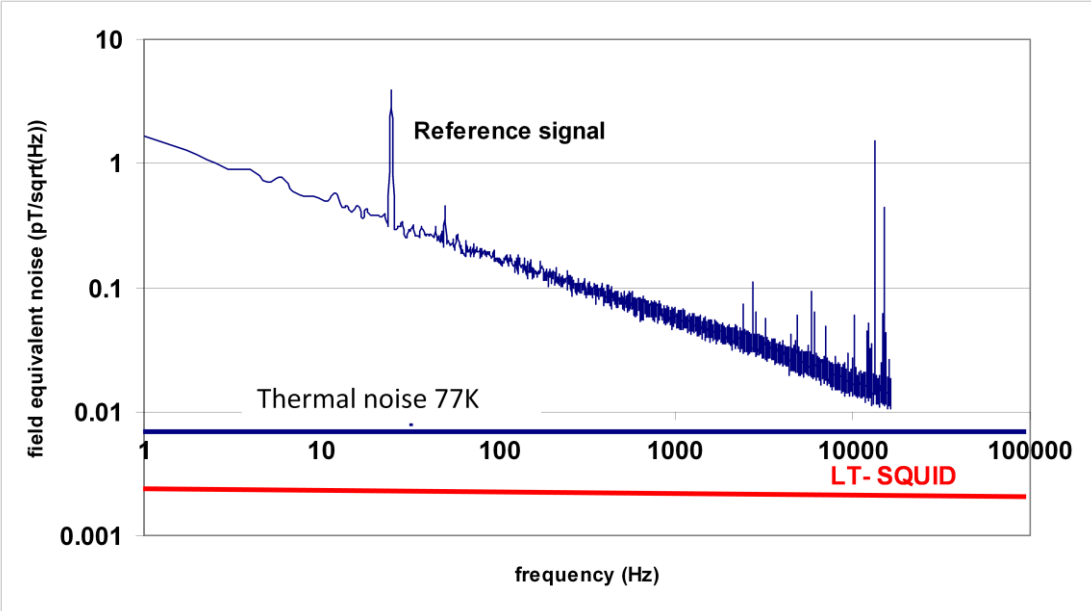

Figure 17: Field equivalent noise recorded in the MSR with a YBCO sensor at 77 K, and with a reference signal of 5 pT at 30 Hz produced by a small dipolar coil. The thermal noise of the sensor is indicated by the plain blue line. Low-Tc Squids detectivity level is indicated by the red plain line.

The noise figure provides useful information on the signal-to-noise ratio for various frequencies. Best performances are obtained in the thermal regime, leading to values of few fT/√Hz (see Table 3). At lower frequencies, the noise is dominated by a 1/f contribution, which reduces the detectivity of the sensor to few hundreds of fT/√Hz.

Sample	Measured gain	Surface (mm^2)	Maximum sensing current	Sensitivity at 77 K (fT/√Hz)	Sensitivity at 4 K (fT/√Hz)
Nb A	108	7x7	1mA	n.a.	600
Nb B	500	15x15	1mA	n.a.	140
YBCO A	160	9x9	15mA	150	32
YBCO B	600	17x17	10mA	25	5
YBCO C	1300	25x25	10mA	8	1.5

Table 3: Detectivity level in the thermal noise regime for various sensors at various sensing currents.

Mixed sensors for low frequency measurements

(The results shown in this chapter –MCG and 1/f noise reduction techniques- are part of the PhD work of Hedwige Polovy)

Low frequency response; sensitivity

Estimated etectivity levels for a YBCO sensor with a gain 1000 are given in Table 4.

Sensor	Noise at 1 Hz	Noise at 10 Hz	Noise at 1 kHz	Noise at 10 kHz
YBCO 4K 100mW	100 fT/√(Hz)	30 fT/ √(Hz)	3 fT/ √(Hz)	2 fT/ √(Hz)
YBCO 4K 1mW	100 fT/ √(Hz)	30 fT/ √(Hz)	20 fT/ √(Hz)	20 fT/ √(Hz)
YBCO 77K 100mW	300 fT/ √(Hz)	100 fT/ √(Hz)	10 fT/ √(Hz)	5 fT/ √(Hz)
YBCO 77K 1mW	300 fT/ √(Hz)	100 fT/ √(Hz)	40 fT/ √(Hz)	40 fT/ √(Hz)

Table 4: Estimated detectivity levels for a YBCO sensor with a gain 1000 at 4 K and 77 K, for various frequencies and current sensing. 100 mW (1 mW) corresponds to 10 mA (resp.1 mA) in a typical 1 kOhm GMR.

Flux jumps and vortex avalanches

In some ramping field experiments, when the field is swept rather quickly, some instability can be observed in the MR response (see Figure 18 left), which corresponds to a flux jump or vortex avalanche phenomenon. We can describe these observations using a diffusion model of the vortices and determine the energy dissipated by one vortex through the constriction.

When the magnetic field is applied perpendicular to this ring, a supercurrent appears to prevent the entrance of the magnetic flux in the loop. This effect is limited by the critical current in the small constriction. When the field is increased over this limit, the supercurrent is still limited to its critical value and some flux can enter in the loop. The entrance is done by vortices crossing the point of the loop where the critical current density is firstly reached, i.e the constriction. The number of crossing vortices and their flow are accurately controlled by the applied magnetic field. If the vortex flow is large enough, the dissipated energy is sufficient to warm locally the constriction until the transition temperature of the constriction is reached; this is a local flux jump. The magnetic sensor allows us to monitor the evolution of the supercurrent as a function of time and applied field.

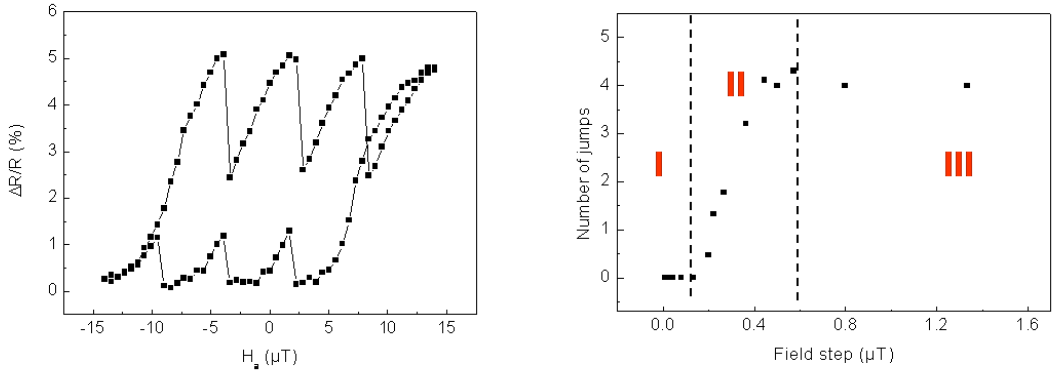

Figure 18 : Left: Voltage variation in the MR for an applied field of -15/+15 µT/-15 µT scanned on 100 points. The corresponding field step is 0.6 µT. Right: Number of jumps as a function of the field step applied to the sample for the Nb-B device. The field has been scanned between -10 and +10 µT at different rate.

When the magnetoresistance reaches the maximal value which corresponds to the critical current in the constriction, a sufficiently high and fast increase of the magnetic field induces a transition to the normal state in the constriction which destroys the supercurrent; this effect is detected by a sudden drop of the GMR resistance. After the resistance drops, the constriction returns to the superconducting state in a very short time. If the field is further increased the same effect can occur again. The same phenomenon has been observed on different size samples.

As shown in Figure 18, during a cycling of the applied field, drops occur several times, always followed by an increase of the MR to the saturation. If the MR curve is not perfectly centered, the height of the drop can be different on the upper and lower plateau.

An important parameter in the occurrence and frequency of the drops is the slope of the applied field. This aspect has been studied by changing the height of the field steps (see Figure 18 right). The duration of the steps, monitored by a GHz oscilloscope, is of 500 ns, independently of the step height.

It appears that for steps smaller than 0.15 µT (equivalent to field sweep rate below 0.3 T/s), the system is stable and no drop occurs (area I). In the range of 0.15 µT to 0.45 µT (0.3 to 0.9 T/s), the number of drops increases roughly linearly with the field step height (area II), and then reaches a plateau corresponding to the maximum number of drops possible within a cycle (area III), taking into account the field necessary to reach the critical state again. For higher values, the number of drops increases to reach its maximum value, given by the total applied field divided by the field required to reach the plateau.

In order to understand this dispersion of energy we have modeled the temperature behavior when the vortices cross the constriction. The heat diffusion equation as a function of temperature T and position r is given by:

$$C(r,T)\frac{\partial T}{\partial t} = \lambda(r,T)\Delta T - (T - T_0)\frac{h}{d} + P(r,T) \qquad \textbf{(19)}$$

where C is the heat capacity, λ is the heat conductivity, h is the heat transfer coefficient at the interface, d the thickness of the Niobium. P is the power brought by the motion of vortices in the constriction. The heat capacity per unit volume is temperature dependent and varies as $C(T) =$

$40.3\,T + 29.3\,T^3\,J.K^{-1}m^{-3}$, leading to $C(4.2) = 2340\,J.K^{-1}m^{-3}$ at 4.2K. The heat conductivity depends on the quality of the niobium and varies with temperature as $T^{2.5}$. From the variation of resistivity from room temperature to low temperature of our sample, we obtain that $\lambda(T) = 0.11\,T^{2.5}$. The heat transfer coefficient has been experimentally determined to be equal to $1.2.10^4 W.m^{-2}.K$. From this model, we can estimate the temperature distribution (Figure 19) in the constriction according to three main scenarios: the vortices are passing along one centered path (scenario 1), along two lateral paths (scenario 2) or homogeneously through the constriction (scenario 3).

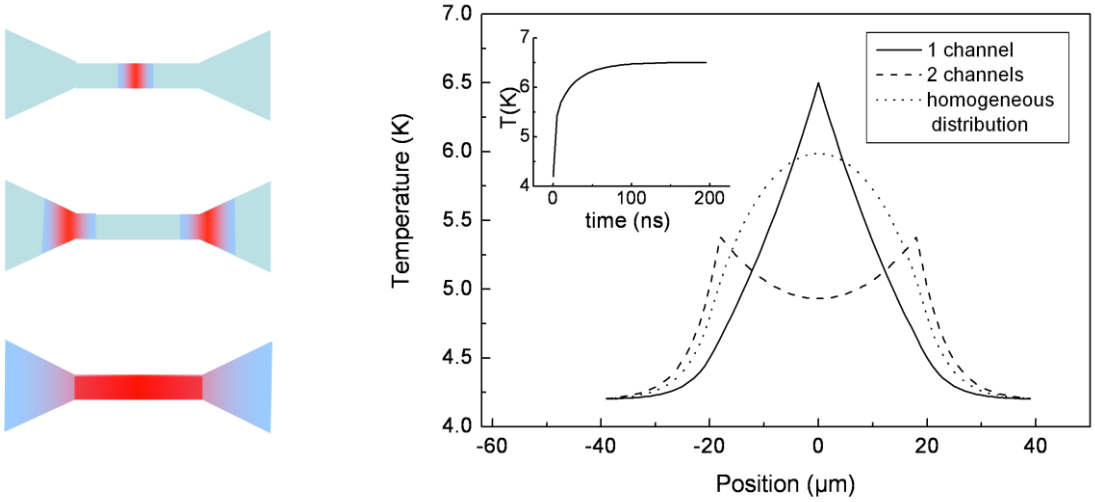

Figure 19 : Temperature distribution in the constriction obtained from a heat diffusion model, for a dissipated energy of 2.15 10^{-12} J, when the vortices cross the constriction on a single channel centered (plain line/upper scenario), when the vortices cross along two different channels located at the edges of the constriction (dashed line/middle scenario) and when the vortices are homogeneously distributed along the constriction (dotted line/bottom scenario). The inset shows the increase of temperature as a function of time.

From our results, we know that the probability to warm the constriction at a temperature higher than 6.5 K is non zero when more than 15 000 vortices (0.15 µT of extra field applied to the inner surface of the loop) pass within the 500 ns of the field ramping time. We can then deduce that the energy dissipated by each crossing vortex is about 1.4x10^{-16} J for a 5 µm path, i.e. 2.8x10^{-11} J.m^{-1}.

It is also important to note that the simulation predicts a constant value for the maximum temperature after only 50ns. This implies that if the experiment time is larger than 50ns, the good parameter for the stability of the constriction is not the total number of vortices but the number of vortices per second. We can give a critical speed of 3x10^{10} vortex/s, corresponding to a speed of 0.3 T/s on the main loop. This value is comparable with the field sweep rates of flux jumps observations [14]

For applications, as long as the sensor operates in its linear response regime, and far from the critical current, no flux jumps occurs and the device exhibits no loss of history. In the case of a fast and strong magnetic field is applied (for an NMR experiment), flux jump can occur, leading in Nb device to a reset of the sensor, which is desirable.

This phenomenon has been rarely observed in YBCO devices, even close to T_c, since the heat capacity is much higher than in Nb. Other hysteretic behavior might be observed in these devices, which will be described later.

Biomagnetic signal detection

Biomagnetic signals

Very sensitive magnetometers operating at low frequency are potential candidates for biomagnetic signal measurements. These signals having weak amplitude (few tens of fT to few hundreds of pT), occur at low frequency (1 to 1000 Hz) and are complex, requiring sufficient dynamics (typically more than few kHz). Their detection is therefore very challenging.

Two kinds of biomagnetic signals are of particular interest: magnetic cardiac signals and magnetic neuronal signals. Both of them are generated by the field lines due to the electrical currents circulating in the heart and in the brain neural networks. In both cases the sources are not unique and the resulting field is non uniform, depending on the location and of the distance to the source.

Cardiac signals:

In the case of the heart, the signal is due to electric ionic currents in the myocardial membranes, spreading and flowing through the tissues, resulting in electric potentials which can be measured by means of chest electrodes (electrocardiography or ECG) or magnetic fields sensors (magnetocardiography or MCG). The ventricular action potential (AP), measured by ECG through the resulting voltage, or by MCG through the induced magnetic field (Figure 20) presents shape and duration characteristics of the ventricular repolarization (ST segment, T wave, QT interval).

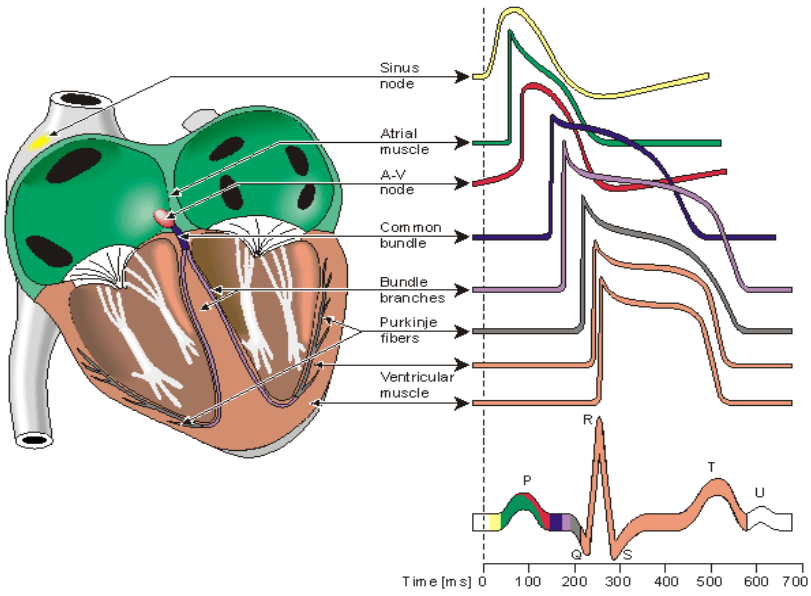

Figure 20 : Schematics of the propagation of the electrical signal in the heart, and resulting electrical component versus time as can be measured on ECG electrodes (from [17]).

First human MCG have been recorded in 1963 by Baule Mc Fee [18] with a set of copper coils and real-time MCGs have been achieved thanks to low-Tc SQUIDs in 1970 [19] . Since then, mapping systems have been developed, allowing vector reconstruction in time. This technique is

complementary to the widely used ECG. It provides more information on specific dysfunctions like ischemia, which may not be properly detected in ECG. As no electrodes are used, this technique presents a non negligible advantage in burns unit. Furthermore, active research using MCG is purchased for the third semester pregnancy cardiac monitoring, where cardiac anomalies are difficult to detect (at this stage, the fetus is protected by the vernix caseosa which is an insulating grease and does not permit recording of the electrical signal via ECG electrodes). Even though MCG systems are much more expensive than ECG and require often a shielded environment, the mapping function and non contact aspect represent large potentiality for systematic population studies. A system which would combine MCG together with non invasive anatomic information (ultrasound or low-field MRI) would be a great tool in hospital environment.

Neuronal signals:

Neuronal activity produces a constant flow of information generated and carried through electrical signals via neurons and synapses. Neural signals are coded in frequency modulation of Action Potential (AP) occurrences. The duration of the AP is of 2-3 ms, with typical frequencies of 0.1 to 100 Hz, propagation speed being of the order of 100 m/s. Like for the cardiac signals, electrical neural signals can be recorded with electrodes on the scalp (electro-encephalography or EEG). The propagating AP is generating some magnetic field lines which can be detected outside of the brain since the human body is transparent to magnetic fields. Magneto-encephalography (or MEG) consists in recording this signal through extremely sensitive sensors (commercially only low-Tc SQUIDs are used for this purpose) usually arranged in arrays of sensors, up to more than 300 devices, in magnetometer and/or gradiometer configuration. They allow getting information on the magnitude and vector components of the field. Solutions to the inverse problem must be obtained to localize the source and get the relevant information (position, feature, time evolution).

In MEG, the sensors are more sensitive to tangential sources, whereas in EEG, radial sources give the dominant signal. The information obtained by both techniques are therefore different depending on the location of the source (sulci or gyri for instance).

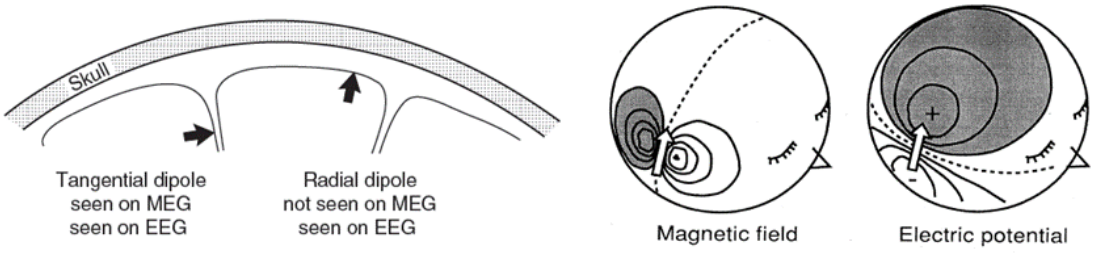

Figure 21 : Left: two type of dipoles, oriented tangentially to the skull (in the sulci) or radially (in the gyri) which can be seen both in EEG, whereas MEG only sees the tangential source (from [21]). Right: Magnetic field and electric potential patterns produced by a tangential dipole (arrow) (from [20]).

MEG is used in clinical and cognitive research. Presurgical mapping of the functions of the brain can be used prior to surgery in some cases of strong epilepsy. Widely used in cognitive sciences, MEG allows temporal information on the normal and pathologic brain functioning. Studies about language, memory, consciousness, sensory-motor functions have been carried out on adults and children. Population with a neurological disorder such as schizophrenia, dementia, Parkinson, Alzheimer, just to cite few, have been studied with this tool.

Precise information in time (in the ms range) and location (few mm^3) are the main advantages of this non invasive technique, applicable on wide range of population. This is nowadays one of the major tools with functional MRI to study the human brain functions.

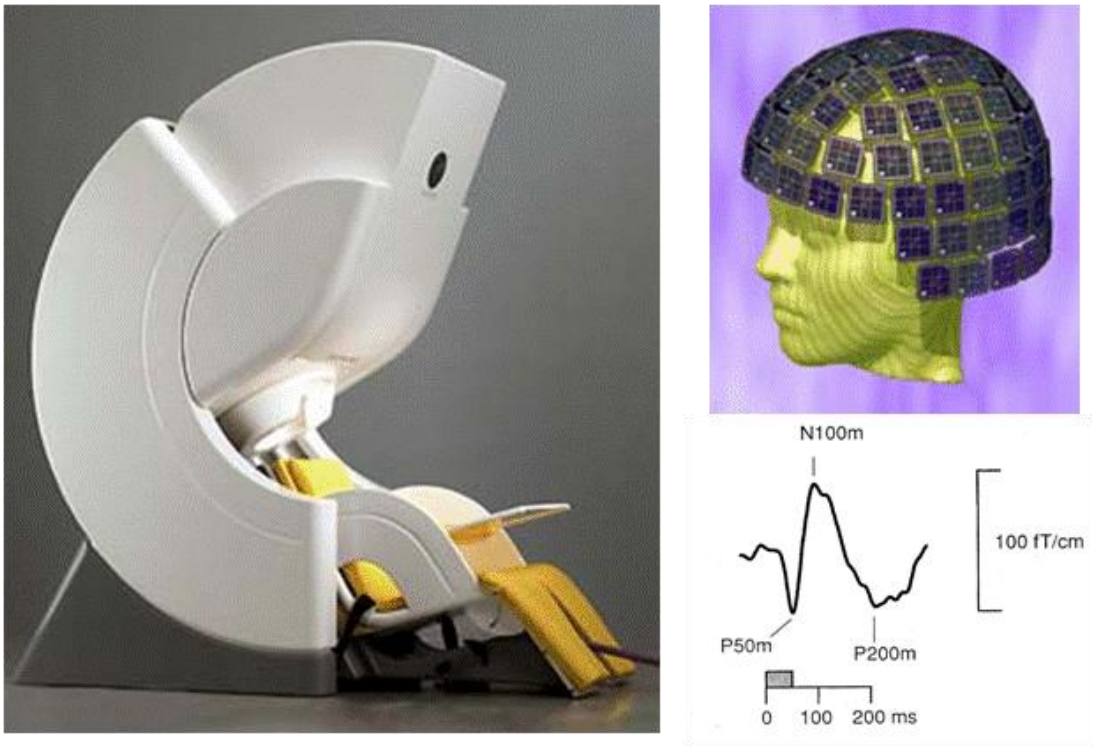

Figure 22 : Left panel: commercial MEG system produced by Elekta Neuromag; Right panel: Top: schematics of the 306 SQUID devices around the head of the subject in the Elekta system. Bottom: typical magnetic response to auditory stimuli of 50 ms (hatched area), measured close to the subject's auditory cortex (from [20]).

First biomagnetic measurements with a mixed sensor

As our sensors have demonstrated noise level of less than 1 pT in the 1/f regime (see Figure 17), it is possible to apply them to MCG signal recording. Due to the very small amplitude of the signals with respect to the environmental noise, it is necessary to operate the experiment in a shielded environment. The experiments have been carried out in the Magnetic Shielded Room (MSR) at Neurospin MEG facility with Nb and YBCO-based mixed sensor. The cryostats used for these experiments are home-made fiberglass dewars, where the sensor is directly placed in the cryogenic liquid (helium or nitrogen). Schematic of the experiment is given in Figure 23.

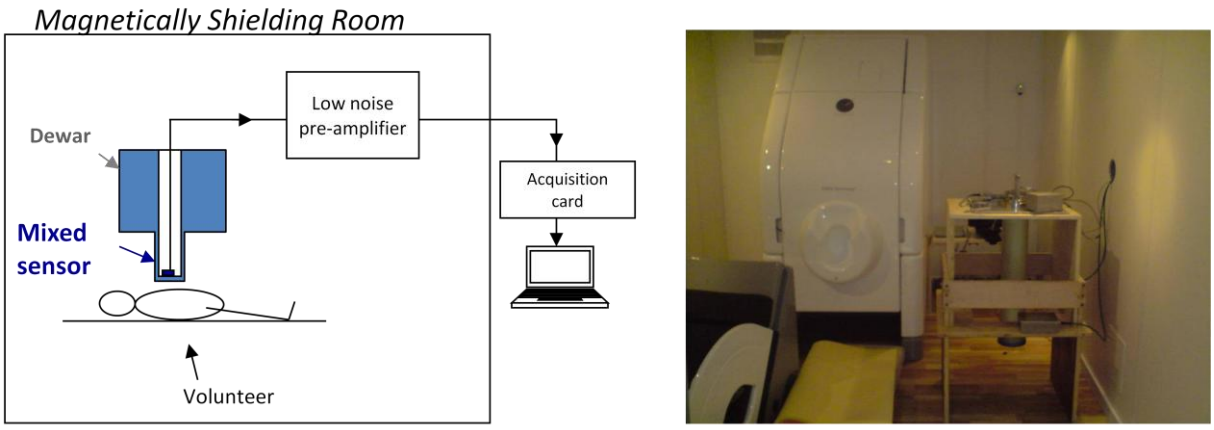

Figure 23 : Left: Schematic of the MCG experiment. Right: Picture of the experimental setup (fiberglass dewar and low-noise amplifier) on the right in Neurospin MSR. The commercial MEG system is visible on the left of the picture.

Simultaneous recording of the ECG with chest electrodes have been done. Raw signals and averaged signals are given in Figure 24 and Figure 25.

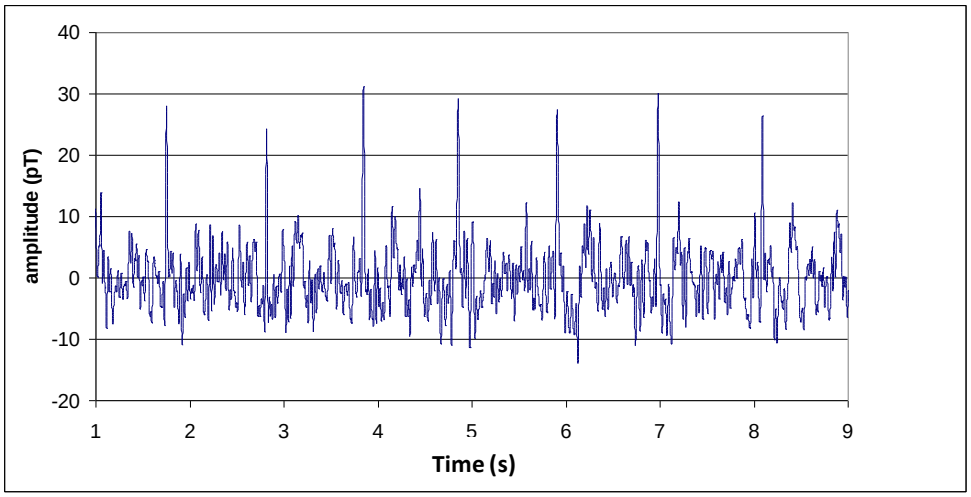

Figure 24 : Raw MCG signal recorded on a Nb-mixed sensor with a thermal noise of 100 fT/√Hz.

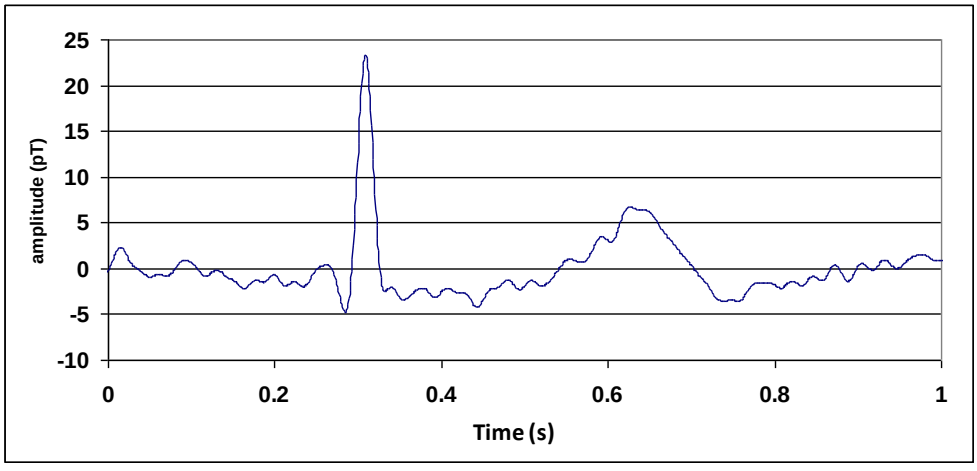

Figure 25 : Averaged (30 times) MCG signal. QRS complex and T-wave are well visible.

Similar experiments have been performed with high-T_c mixed sensors at 77 K, demonstrating the performances of the sensor in this range of field and frequency.

Recording (also) the artifacts and ballistocardiography

As mixed sensors are sensitive to any magnetic field present in the environment, it occurs sometimes that during the experiment some artifacts generate signals stronger than the MCG signal. One common artifact is the presence of a ferromagnetic contaminant on the subject, for instead slightly magnetic ECG electrodes. In this case, a large and slow oscillation, fitting to the breathing of the subject, induces a very low frequency signal (Figure 26) corresponding to the motion of the contaminant.

Another artifact, more difficult to identify may occur, which is due to ballistocardiography (BCG). When the heart beats, the blood flow sent by the artery to the ends of the body induces a very small motion of the body itself, at a frequency of a cardiac pulse, i.e. at the same frequency as the electrical heart signal. This is the ballistocardiographic effect [22] . If a ferromagnetic material is present on the clothes or on the body of the subject, this pulsed motion of the body will induce a motion of the small magnetic object. One way to identify it is that this artifact will show various patterns when changing the sensor's position (Figure 27).

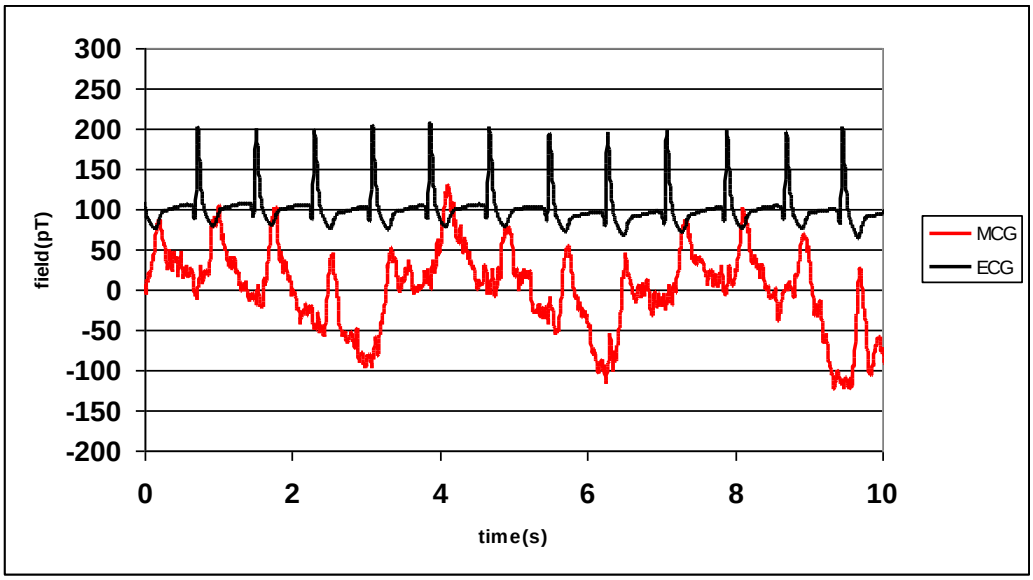

Figure 26 : Raw ECG (black) and MCG (red) data recorded simultaneously. The strong oscillation in the MCG corresponds to the breathing of the subject. This is probably induced by the motion of small ferromagnetic material present on the subject (here probably the ECG electrodes).

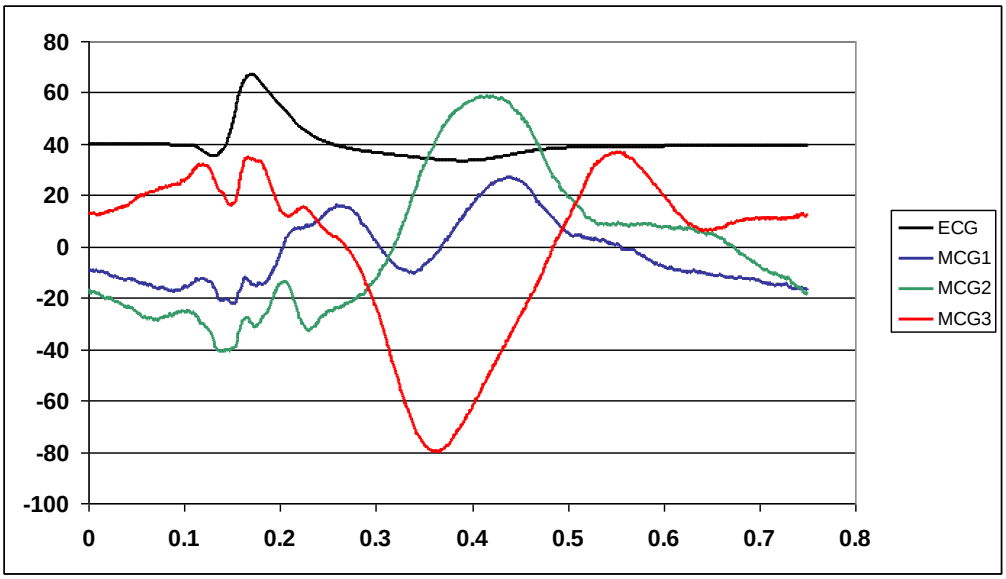

Figure 27 : MCG signals for various locations of the sensor over the subject's torso. The magnetic patterns, very different from one position to another is due to the presence of a ferromagnetic contaminant (i.e. nickel pants button) which is slightly displaced by the blood heart beat and therefore gives a magnetic signature at the same frequency as the MCG and ECG, but with a complex field line pattern.

Discussion on biomagnetic measurements with a mixed sensor

Limitations to the performances of the devices at this point are the following:

- *Noise of the pre-amplifier:*
  We have used a room temperature low noise preamplifier INA 103, with a thermal noise of 1.2nV/√Hz. For the lowest frequencies (<1kHz), the noise of the GMR elements are strongly dominant (by 1 to 2 orders of magnitude, depending on the frequency), but if the sensor sensitivity increases, the amplifier noise may contribute. Therefore we have started to implement cold preamplifier made out of SiGe transistors provided by Mikko Kirivanta at VTT, Finland. These devices should have an intrinsic noise of only 170pV/√Hz.
- *Environmental noise:*
  The sensors have been used as magnetometers with no reference point. They are therefore sensitive to all sources of external noise, including the residual environmental noise present in the Magnetically Shielded Room. To increase the amplitude of the relevant signal (MCG or later on MEG), one could work in gradiometric mode, with a sensor afar from the source, which would record the residual noise in order to subtract it on the primary sensor (closest to the relevant source). This method is widely used for SQUIDs and in some cases allows working in a lighter shielding environment or no shield at all.
- *1/f noise:*
  As it has been seen in Part II, the main source of noise of the sensor at low frequencies is the 1/f noise. To get sensitivity of tens of femtotesla, needed for MEG, with the present sensors, one should find ways to reduce or cancel this noise. This point is developed in the next section.

1/f reduction techniques

This 1/f noise is given by the GMR element, which is of small volume. In order to reduce this

contribution, modulation techniques can be developed and applied. Simple current modulation would not be effective since the sensor is linear. Modulation of sources cannot be applied due to the nature of the signal sources (biomagnetic sources or NMR signals). Modulation can however be applied by switching the sensor in two configurations, one where the sensor operates and records the signal, and one configuration where the sensor is set to blank. This can be achieved by saturating the sensor or by acting on the state of the superconducting loop of the sensor (open or closed). Indeed if one cuts the supercurrent path in the loop, the sensor will not be sensitive to the applied flux, and will be set to zero change in the magnetoresistance.

Saturating the supercurrent

One idea to modulate the sensor is to reach a reference point. This can be achieved by reaching the critical current in the constriction. At this point, the sensor is not sensitive anymore to any external field variation. One way to achieve this is to apply an extra field which will drive the sensor to the saturated state, but this technique leads to a loss of history of the sensor. Another way is to inject a current in the loop to reach the critical current in the constriction, and so a reference point. It can be very fast and work easily, but the absolute field reference is also lost and the information obtained will be only the derivative of the signal, not the signal itself.

Local heating technique

A local heating of the constriction can be achieved by driving a sufficiently high current on a local point of the constriction (as can be seen in Figure 28). This local heating can be performed in the kHz range, leading to a modulation of the sensor at a frequency which corresponds to the thermal noise. If two constrictions are mounted in parallel, switching on and off the heating of these constrictions leads to a modulation of the supercurrent without destroying it. An example of this modulation is shown in Figure 28. A 30 Hz sinusoidal signal of 100 nT is recorded by the sensor on which an alternating heating is performed. One can see from the experimental curve that the external signal is modulated at the frequency of the heating pulses. Such techniques can get the sensor sensitivity at low frequency to be increased by one to two orders of magnitude. Figure 29 shows the noise measured with and without the modulation.

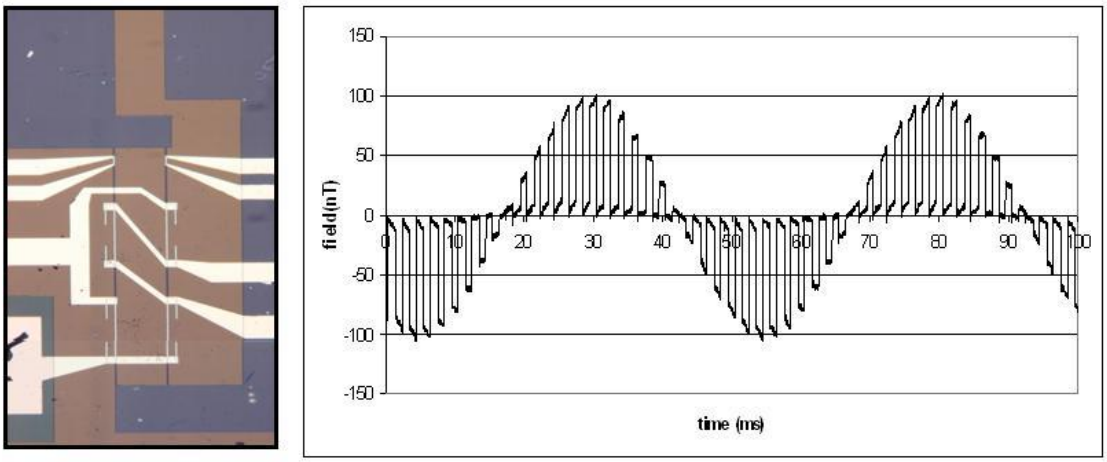

Figure 28: Left: Micrograph of two GMR elements (C shaped) mounted in bridge configuration and heating contact lines. Right: 100 nT peak to peak signal created by a small coil and detected by a magnetoresistive hybrid sensor with a toggle of the supercurrent running in the loop. The curve gives the signal detected by one of the GMR element in the bridge.

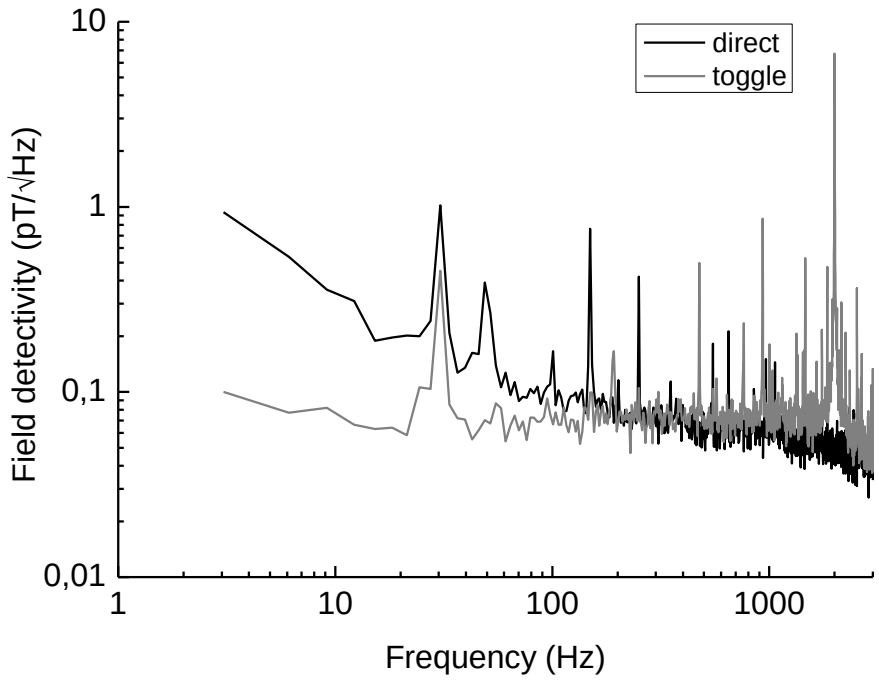

Figure 29: Low frequency noise without (dark grey) and with (light grey) modulation. The peak at 30 Hz corresponds to a test signal in a small external copper coil.

This technique has some drawbacks: the current required to heat the constriction is of several mA or tens of mA, and if the stray fields generated by this current on the superconducting loop can be cancelled by symmetrizing the contact lines, capacitive effect occurs through the insulating layer and the superconductor to the GMR, leading to strong peaks in the magnetoresistance when the heating pulse is on. This effect might be a limitation to the efficiency of this technique.

Another idea therefore is to use a local non electrical heating by a laser probe. Schematics of the experiment is shown in Figure 30.

The laser is a 140 nm pulsed diode which can provide a power up to 1 W. The diameter of the probe at the output (1 mm) can be focused by means of optical lenses to part of the constriction. For this experiment, a new design of the sensor, with a longer constriction is required, but first tests will consist in testing the condition in which the mixed sensor is set to zero and recovers from the laser pulse (duration, power, repetition rate…).

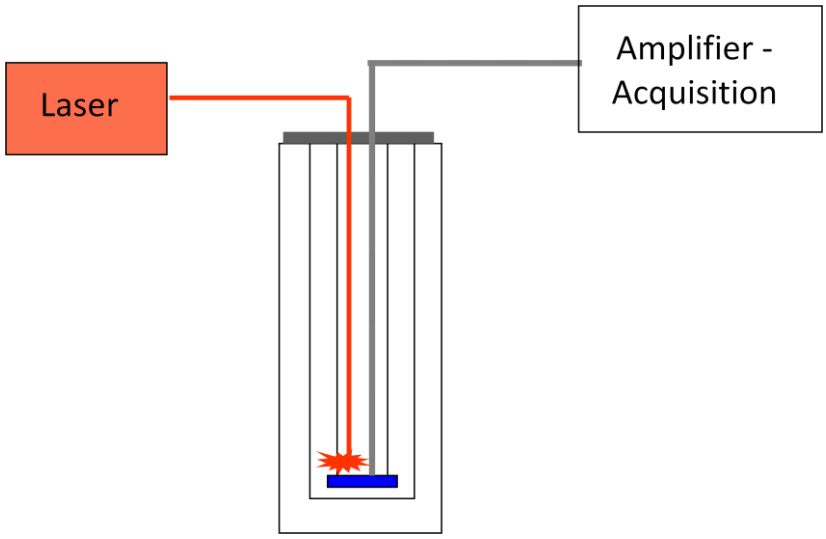

Figure 30 : Schematics of the 1/f noise cancellation technique with a laser probe.

Conclusion

In conclusion of this part on the low frequency range, mixed sensors already exhibit sensitivity in the picotesla range at very low frequency, and can be already applied for MCG recordings. Improvements of the sensitivity at low frequency can be achieved by dedicated modulation techniques, opening road for MEG recordings with mixed sensors at 77 K.

Mixed sensors for resonant signals detection

(The results shown in this chapter are part of the PhD work of Hadrien Dyvorne)

The previous part has been focused on characteristics and application of mixed sensors in a low frequency range (<10 kHz). Here, I address the characteristics of mixed sensors at higher frequencies and present two areas where femtotesla resonant signals can be detected by the sensor: Nuclear Quadrupolar Resonance and Nuclear Magnetic Resonance.

Sensitivity to radiofrequency signals

From the noise figure of the mixed sensor, it clearly appears that the most sensitive range of the device is in the thermal noise, for frequencies typically higher than 100 Hz to 10 kHz –the 1/f knee depending on the GMR composition and of the quality of the stack. For higher frequencies, the limit of detectivity is given by the signal-to-noise with respect to:

$$SN_{Therm} = \beta(T) H_{perp} g \sqrt{P_m \frac{l}{4kT}} \qquad (20)$$

A flat response is therefore expected up to high frequency values. Limitations in radiofrequency response are given by three different elements: the magnetoresistive sensor, the loop itself and the response of the superconductor.

Micron size magnetoresistive sensors have flat RF response until the GHz regime. The limitation is given by the spin wave resonance frequency [23] which is about several GHz for the sensor configuration we are using. Figure 31 gives the response of a GMR sensor as function of frequency. Different regimes can be observed: below the resonance peak, the response is flat down to DC and is given by the static susceptibility of the magnetic free layer. When the frequency is approaching the resonance of the free layer, the MR sensor presents a peak of sensitivity and after the peak, the susceptibility of the free layer decreases rapidly to zero. The most important point is the fact that the response of the GMR sensor can be rather important even if a rather strong magnetic field is applied. This allows using mixed sensors in presence of large fields.

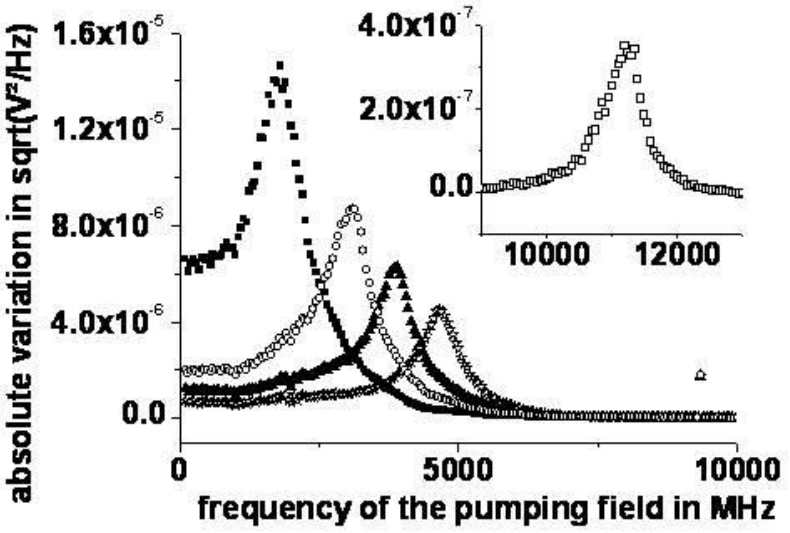

Figure 31: Response of a GMR sensor as function of the frequency for different value of the external field (■ 0 Oe, ○ 50 Oe, ▲ 100 Oe and ★150 Oe). The sensor is fed with a current at 2.005 GHz. The inset shows the measurement for H=1000 Oe [23] .

The superconducting loop is designed to have a minimal inductance in order to maximize the circulating supercurrent. Typical loop of 1cm² presents an inductance of about 100 nH. If the mixed sensor is built on an insulating substrate, the residual capacitance is very low, pushing the self resonance of the loop far above the RF detection.

The last limitation should be given by the superconductor itself but as it is a superconducting loop in the Meissner regime, without any junction effect, we should not see any limitation at frequencies lower than hundreds of MHz.

We have experimentally tested the response of a mixed sensor to a RF field until 10 MHz and obtained a constant sensitivity on the whole range.

Detection of a resonant signal

Nuclear Magnetic Resonance experiment

Detection of magnetic resonance of nuclei with non zero spins can bring powerful information on the chemical composition and environment of a compound. In presence of an external applied magnetic field, the energy levels of the nuclear spin are split due to the Zeeman interaction. At a given temperature, the difference of population between the two levels is given by the Boltzmann's law. This difference creates a non zero magnetization which can be detected. This magnetization is proportional to the external field and is given by:

$$M_0 = \frac{N\gamma^2\hbar^2 B_0}{4kT} \qquad (21)$$

where γ is the gyromagnetic factor (42.57MHz/T for the proton), B_0 the external field and N the number of nuclei in the sample.

At equilibrium this magnetization is along the applied magnetic field. A RF pulse field applied perpendicularly to the main magnetic field at a frequency corresponding to the energy splitting induces a rotation of the magnetization.

Then the magnetization starts precessing around the direction of the static field and relaxes to equilibrium. The precession pulsation is given by the Larmor's law:

$$\omega_0 = \gamma B_0 \qquad (22)$$

The important parameters that govern the efficiency of detection for a given nucleus are its concentration, the resonance frequency and the relaxation times T_1, T_2* and T_2. T_1 is the longitudinal relaxation time and it characterizes the return to equilibrium of the system. T_2* is the loss of coherence of the spin precession including extrinsic factors such as inhomogeneities (field, temperature…) inside the sample. It can be also seen as the time inverse of the resonance line width. T_2>T_2* is the intrinsic transversal relaxation time i.e. the loss of coherence of the spins in general due to spin-spin interactions.

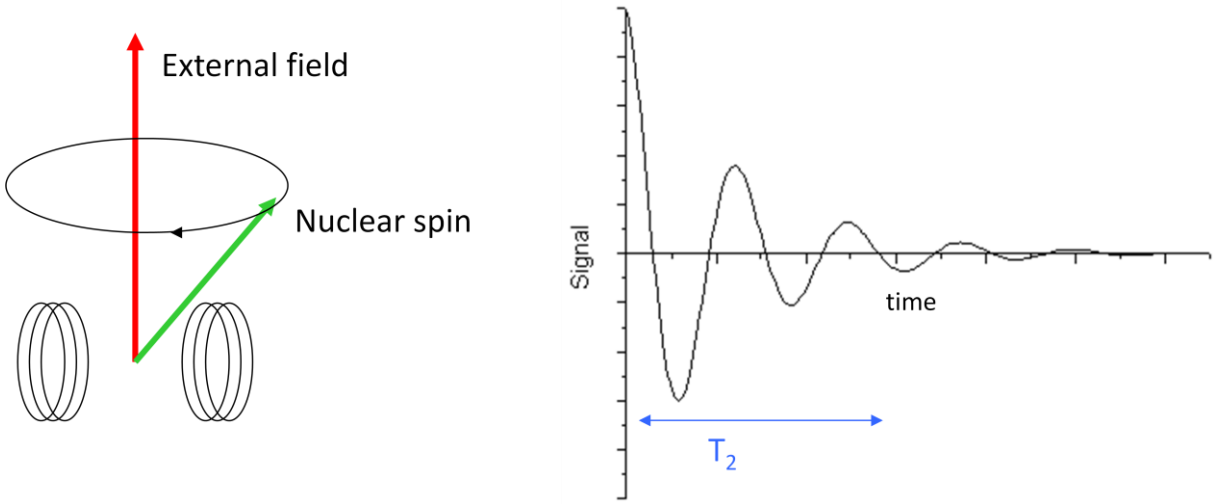

Figure 32: Left: Schematics of an NMR experiment, the nuclear spins precess around the direction of the static field after the RF pulse has been sent. Right: NMR signal as a function of time, T_2 being the relaxation time.

In a resonant experiment, the spins are polarized by the static field and experience an RF pulse at the required frequency. In a classical scheme of detection, the precession of the nuclear magnetization at the resonance frequency after the pulse is detected through a voltage induced in a coil by the Faraday effect (Figure 33). Usually the same coil is used for excitation and detection.

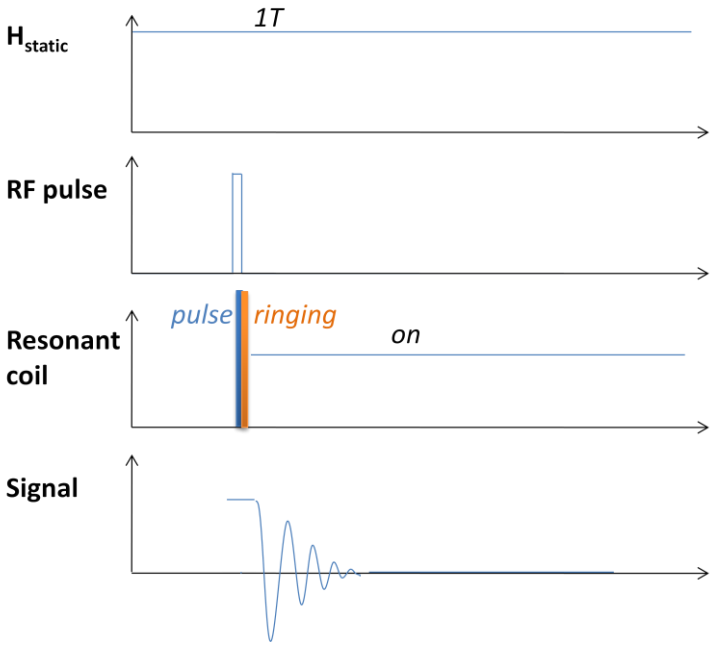

Figure 33: Schematics of a classical high-field NMR experiment. The static field is always on, the resonant coil is used to send the RF pulse and to detect the resonant signal. Shortly after the pulse, the coil is ringing from the pulse saturating the preamplifier. The NMR free induction decay signal is visible after.

The strength of this signal depends on the magnetization, which is directly proportional to the value of the static field (eq 21). This is the reason why conventional NMR and MRI experiments are carried out in high fields (several teslas). Furthermore, at higher fields, the corresponding resonant frequency is in the hundreds of MHz range and can be detected by resonant coils whose sensitivity increases with frequency.

Operating at high fields present anyhow some limitations, which are mainly due to the difficulty of having a very homogeneous field over the volume explored and to reach tesla-range stable fields. This is usually achieved with superconducting magnets, requiring liquid helium environment and leading to expensive apparatus.

Low field NMR and MRI

There is therefore a strong interest in detecting resonant signal at lower fields (i.e. at lower frequencies), even if the signal decreases due to the small polarization. Such experiment applied to MRI can lead to lighter, cheaper apparatus, and allowing measurements on population up to now excluded (metallic objects are then accepted without safety issues). Measuring signals in the MHz range or lower can hardly be addressed by resonant coils, which become less sensitive. Other type of sensors in the femtotesla range are then required. SQUIDs are the best candidates so far due to their sensitivity and to their response flat in frequency up to hundreds of MHz.

The use of SQUIDs in ultra low field NMR and MRI has been intensively investigated [24] and the coil sensitivity and SQUID sensitivity overlap between few 100 kHz and 4 MHz, depending on the sensor geometry [25] The common technique for SQUID detected NMR is based on the prepolarization of the sample in an inhomogeneous field of 1-100 mT and subsequent detection at ultra low fields (50 µT). The procedure presents the advantage of increasing strongly the signal by increasing the magnetization but it is necessary to protect the SQUID which is generally not field tolerant above few

mT. The counterpart is a longer acquisition time and the difficulty to proceed with multipulse sequences like Spin-Locked-Spin-Echo (SLSE) we have used for NQR.

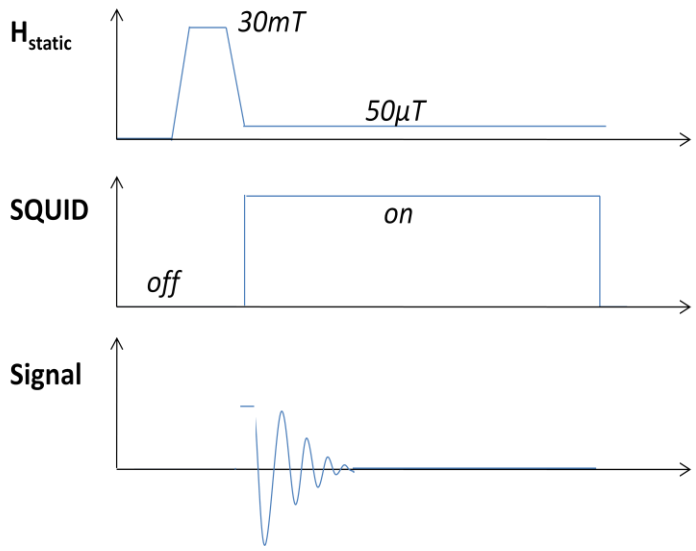

Figure 34: Schematics of a low-field NMR experiment with a SQUID. A prepolarizing field of few tens of mT is applied as well as the RF pulse. The field is reduced to its measuring value (typically tens of µT) and the SQUID can then be switched on to measure the signal.

Mixed sensors and resonant signal detection

Mixed sensors having also a large bandwidth and exhibiting a flat response in frequency, they can be advantageously used in resonant signal detection.

In a first experiment, we have measured the mixed sensor readout in a NMR-like experiment where an RF pulse of 1 kW is applied during 50 µs then switched off. Experimental data are presented in Figure 35.

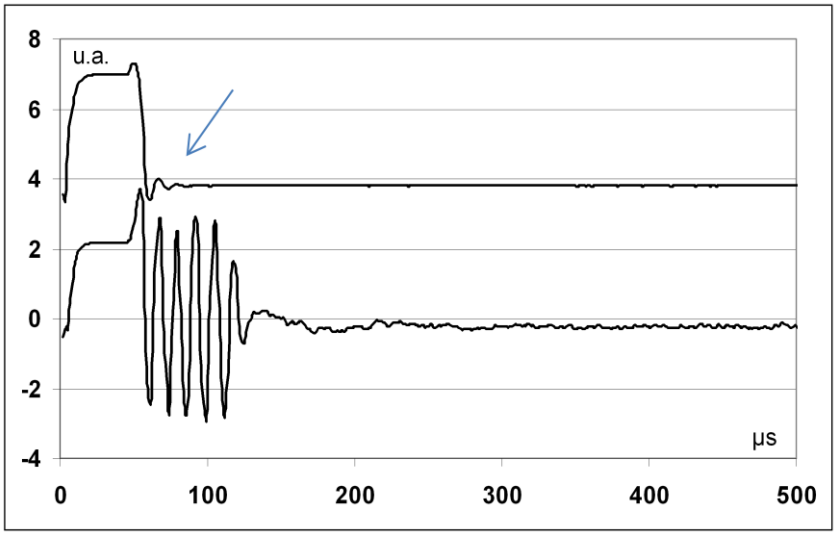

Figure 35: Response at 800 kHz of the same signal with a mixed sensor (upper curve) and with a resonant coil (lower curve). The duration of the pulse is 50 µs. The mixed sensor is operational just after the pulse and in classical NMR the ringing time of the coil saturates the spectrometer for 60µs. The reception frequency has been shifted by 50kHz for a better view of the ringing oscillation. The resonant oscillation at 800 kHz can be seen on the mixed sensor (indicated by the arrow).

The pulse has two effects: a heating of the full sensor and a magnetic saturation of the GMR element. Nb and YBCO based mixed sensors exhibits different behavior. For Nb based mixed sensor, the heating of the constriction is sufficiently high to reach the critical temperature transition of the Nb and then the mixed sensor is reset. As soon as the pulse is finished the constriction cools down and the mixed sensor is ready to measure, back to the zero supercurrent state. The sensor is fully operational after a time shorter than 0.3 µs. From the simulation of the cooling of the constriction taking into account the heat capacity and the various thermal conductivities, we can determine a cooling characteristic time of 50 ns. For YBCO based mixed sensors, the critical temperature is not reached. The supercurrent oscillates at the RF frequency from minus the critical current of the constriction to plus the critical current of the constriction and when the pulse is finished, the mixed sensor is in state with a supercurrent equal to the value at the end of the pulse. This case is slightly less favorable because depending of the value of this supercurrent, the GMR resistance can be different inducing a small dephasing of the NQR signal but this effect is rather negligible.

If we observe the behavior of a Nb sensor (Figure 35), it appears that the sensor is tolerant to the strong RF pulse, during which it is saturated. Just after the pulse is switched off, the sensor is operating and in the case of our experiment already records a small resonant signal at 800 kHz. We have recorded the resonant coil response meanwhile, and we can observe the large oscillating signal of the coil due to the ringing. As the mixed sensor is untuned, no ringing occurs.

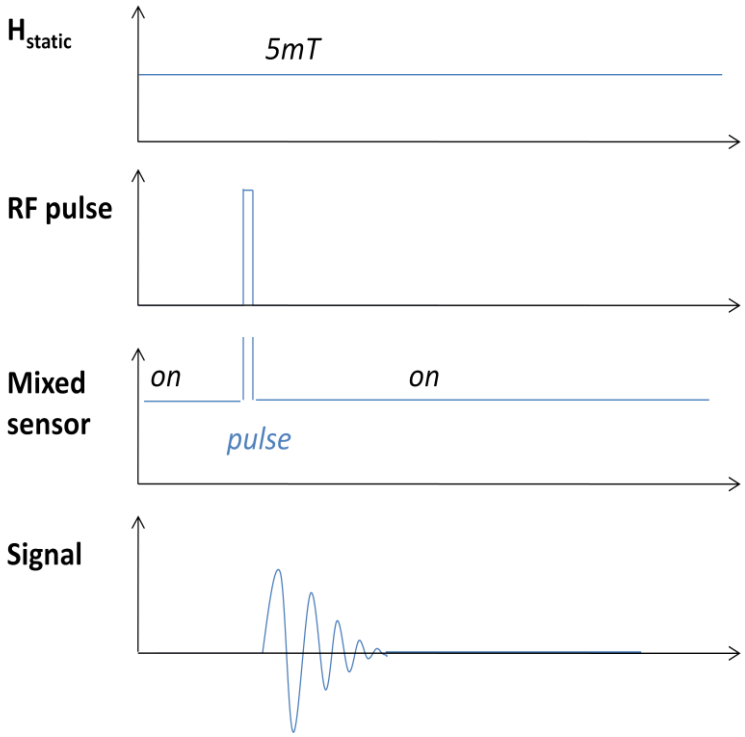

Figure 36: Schematics of an NMR experiment with a mixed sensor where a static field of few mT is continuously applied. The sensor is blinded during the RF pulse but recovers extremely shortly after (100 ns). This experimental configuration allows multiple complex sequences or slicing in MRI.

Therefore we can build two type of resonant signal detection with mixed sensors, one with a prepolarizing field (like for SQUIDs), the other in a configuration where the static field is applied during all the experiment, which allows performing more complex sequences (SLSE) and reducing the

total acquisition time. In the latter experimental setup, the static field should not exceed few mT, otherwise the GMR element would be saturated, and this static field cannot be applied directly perpendicularly to the sensor. Saddle coil configuration may be well suited for this experiment.

Nuclear Quadrupolar Resonance and explosives detection

Nuclear Quadrupolar Resonance

Nuclear Quadrupolar Resonance (NQR) is a solid state spectroscopic technique that applies to nuclei of spin I≥1 in a non cubic environment. Nuclei with an electric quadrupolar moment, such as ^{14}N, ^{35}Cl and ^{63}Cu, have their energies split by an electric field gradient, created by the electronic bonds in the local environment. The resonance frequencies are compound specific and allow detection of various kinds of objects (explosives, drugs, oil...) on the basis of their chemical composition, which is an important advantage over other methods that detect extrinsic properties such as metallic mine detectors. The technique requires that the substance is in a solid state and that the environment of the nuclei of interest is non cubic, otherwise the electric field gradient is zero because of symmetry consideration in the cubic case, or because of motion averaging in the case of a liquid substance.

Most solid explosives contain an important proportion of nitrogen which allows their detection by NQR. The resonance frequencies lie in the 300 kHz-5 MHz range.

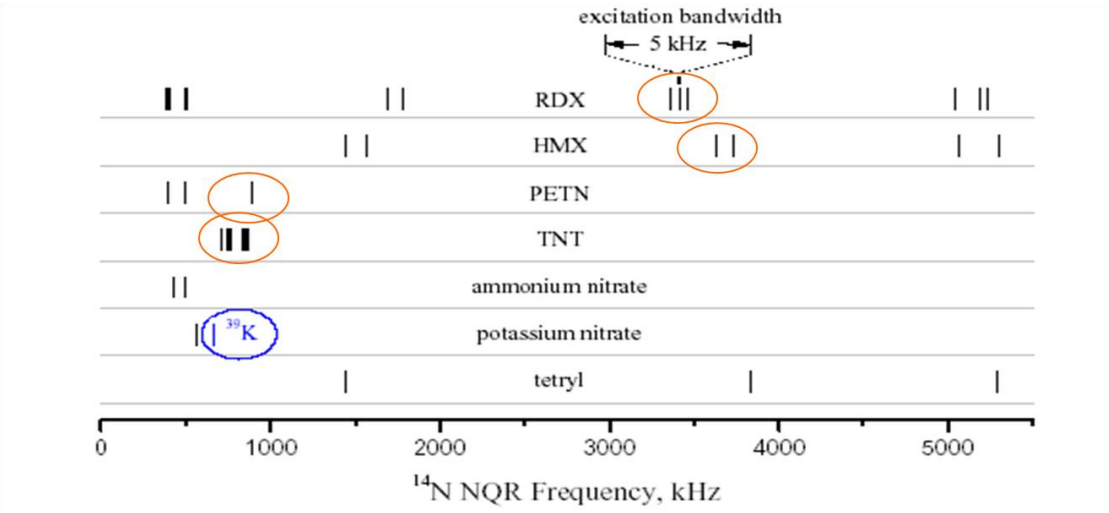

Figure 37: Frequencies of the resonant quadrupolar signal for various compounds used in explosives. (adapted from [26])

The simplest NQR detection experiment consists of an excitation produced by a radiofrequency pulse which induces a rotation of the spin orientation of the nuclei having a resonance at the corresponding frequency. This is the equivalent of the π/2 pulse in NMR. Then the excited nuclei precess and relax to their equilibrium. In the classical scheme of detection, the precession of the nuclear magnetization at the resonance frequency after the pulse is detected through a voltage induced in a coil by the Faraday effect. Usually the same coil is used for excitation and detection. Unlike NMR experiment, no magnetic field is applied to polarize, and the resonant frequency is fixed for one compound.

NQR detection of explosives has until now be widely studied ([28] -[31]). However, NQR systems have until now not really been implemented in real conditions due to the fact that the sensitivity is

still rather low, especially for TNT which presents a low density of Nitrogen and long relaxation times. The limitation in sensitivity is given by the thermal noise of the detecting coil in the range of frequency of the signals (3-4 MHz at most for RDX or HMX, 800 kHz for TNT and At 421 kHz for ammonium nitrate). For that reason, alternative very low noise sensors as SQUIDs [32] or atomic magnetometers [33] are explored. Mixed sensors are also good candidates for this application. Furthermore, usually metallic parts are present in the neighborhood of explosives making difficult their detection by a tuned detector.

Experimental setup

In order to test the response of hybrid sensors, we have mounted a NQR system able to detect ^{14}N resonances in the range of 100 kHz to 10MHz (Figure 38). The spectrometer has a 0.1° phase accuracy, 100dB amplitude control and 10ns pulse resolution. A double frequency change (super-heterodyne reception design) associated to very low noise preamplifiers in the reception part insures an optimized signal to noise ratio of the electronics. The effective noise is mainly given by the thermal noise of the resonant coil or the hybrid sensor+preamplifier. The two preamplifier chains for the resonant coil and the hybrid sensor are simultaneously operational and the acquisition can be switched between each channel. The coils used in the experiments have a solenoid shape (radius = 6 cm, length = 1 cm), and are well-fitted to the volume of the explosive tested, about 80 g. The working distance is between 5 and 10 cm. The hybrid sensor has an additional distance of 2 cm from the explosives. The pulse power was at maximum 500 W. The pulse length was optimized for the best signal.

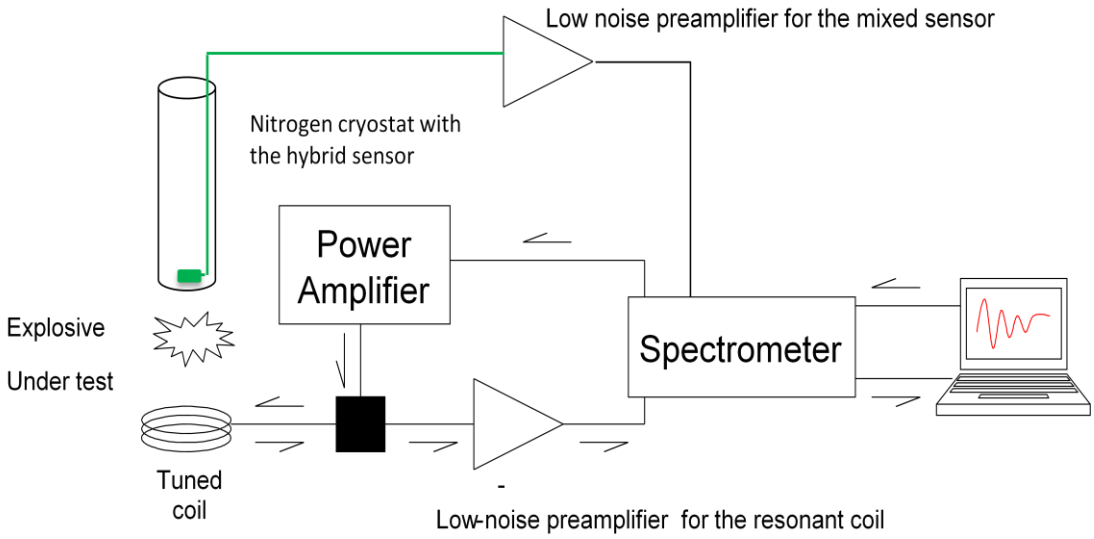

Figure 38: Schematics of the experimental setup. A surface coil is connected to a home-made spectrometer controlled by a PC. It acts as the pulse emitter and a RF receiver. The mixed sensor is placed on top of the explosive and connected to its own preamplifier. The probe and the preamplifiers are separated from the remaining part by several meters.

In another configuration, a pickup coil can be used where the primary loop is wound around the volume where the explosive is located, the secondary loop being located in front of the sensor, with a number of turns chosen to match the inductance of the primary loop and with the size of the superconducting flux transformer of the mixed sensor (see Figure 39). In this configuration, the filling factor is optimized, compared to the previous one but the coupling transformer induces a loss of signal by a factor 3 to 4.

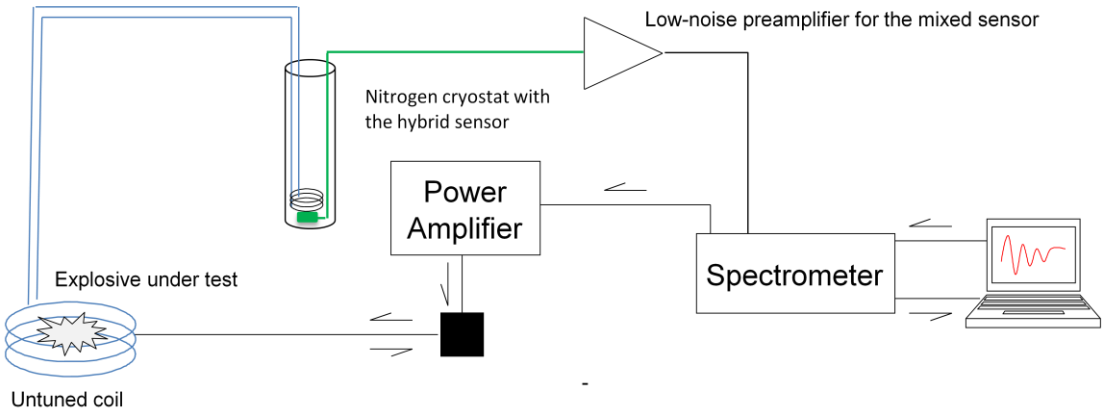

Figure 39: Schematics of the second experimental setup. An unturned coil is wound d around the volume of the explosive. The secondary of this pick up coil is facing the sensor with a number of turns which match the inductance of the primary loop. The pulse is emitted with a power amplifier on the primary of the coil. The mixed sensor is connected through its preamplifier to the spectrometer. In this configuration, the dewar can be positioned at a certain distance (around one meter) of the explosive sensing area.

Detection of explosives

With these experimental set-ups, we have been able to detect various explosives. For some of them (RDX, HMX), detection is extremely fast and a single pulse experiment without or with a small averaging leads to an unambiguous result (Figure 40) but even for TNT which is the hardest compound to detect, a single pulse scheme has been used for determining the relaxation times. For many compounds (TNT, ammonium nitrate, pentrite), the signal is measured with optimized multi-pulse sequence (SLSE) (Figure 41).

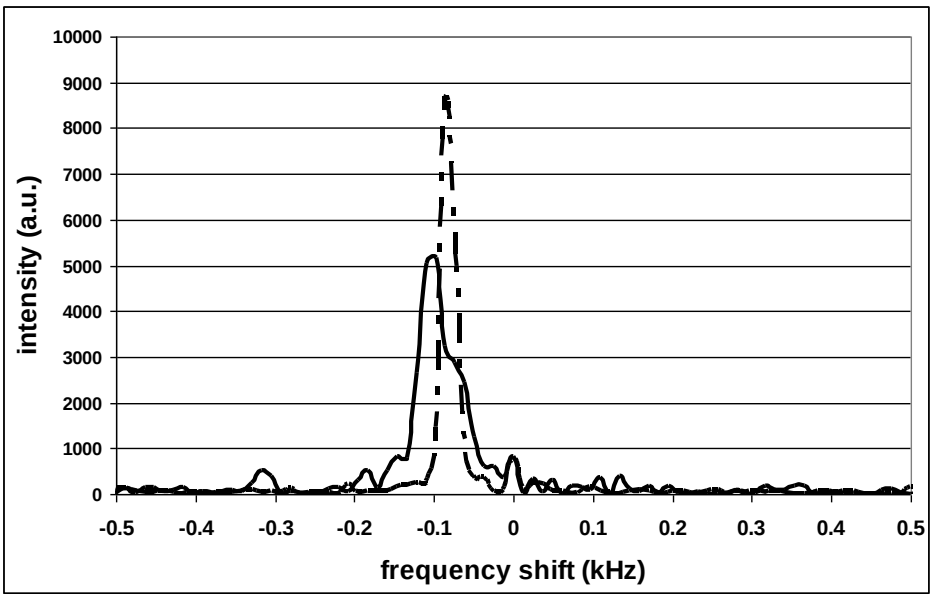

Figure 40: RDX signal detected at 3.4MHz with a single pulse sequence with the resonant coil (continuous line) and the hybrid sensor (dotted line). This signal has been averaged during 10 s. The hybrid sensor used is a Nb-based sensor at 4K. The signal is given in arbitrary units as function of frequency offset in kHz.

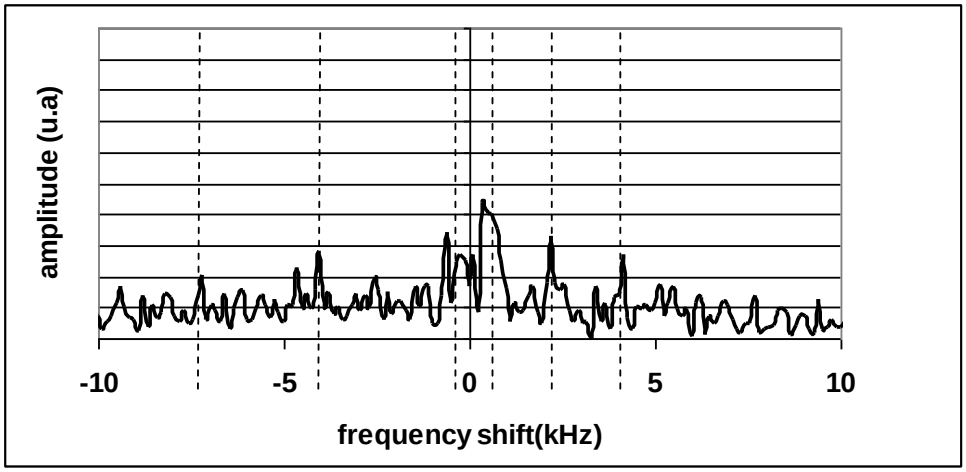

Figure 41: TNT spectrum observed with a single pulse sequence at 842 kHz with a hybrid YBCO sensor at 77 K with a noise of 8 fT/√(Hz) (including the preamplifier noise). Both crystallographic phases monoclinic and orthorhombic are present in this compound. The lowest peak is at 834 kHz (monoclinic phase) and the highest seen is at 846 kHz. Other peaks have been detected at 854 kHz and 868 kHz.

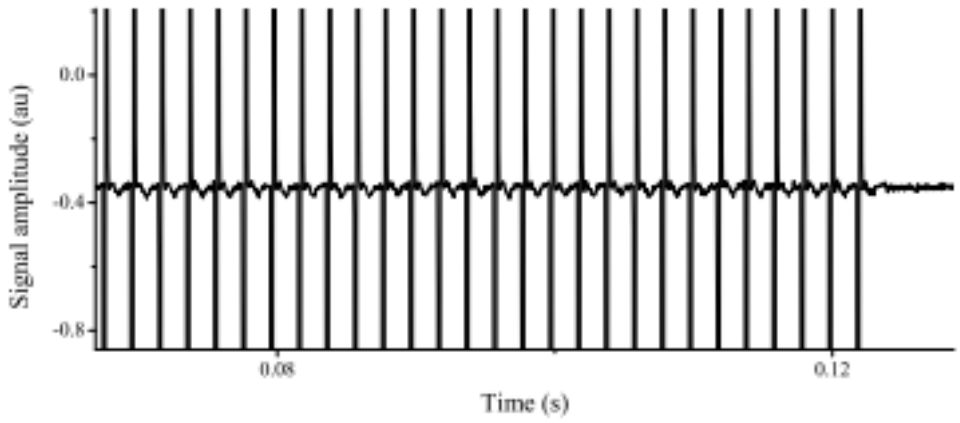

Figure 42: SLSE (spin lock spin echo sequence) on PETN showing the refocusing of the spin signal between each pulse. Averaging of the echoes allows us improving strongly the detection time.

Table 5 summarizes various compounds or compositions we have detected with mixed-sensor NQR, as well as their characteristics.

Composition (Compound)	RDX	HMX	PETN	TNT	Dynamite (ammonium nitrate)
Resonance frequency	3.41 MHz	3.6 MHz	890 kHz	840 kHz	400 kHz
Type of sequence used	Single pulse/SORC	SLSE	SLSE or Echo	SLSE	SLSE
Detection time for 200g	<5 s	20 s	20 s	6 s	10 s

Table 5: Compounds and compositions detected with a mixed sensor, indicating resonance frequency, type of sequence and detection time.

Mixed sensors exhibit a promising way to achieve high sensitivity detection of solid explosives by NQR. Present sensitivity of our sensors gives signal to noise comparable to optimized resonant coils

at 500 kHz, but with a non resonant system allowing simultaneous detection of several explosives. Next generation of sensors with larger size loops and smaller constriction will give us a sensitivity which could be 5 to 10 times better than existing systems. Use of deported pickup coil allows detection over large volumes without increasing the size of the cooling system. A prototype for hand luggage scanning in under construction based on this apparatus.

Very low field Nuclear Magnetic Resonance and Imaging

Second experimental setup we have developed integrating mixed sensor in a low-field MRI detection system.

Experimental set up

The experimental set-up consists of an excitation coil and a pair of Helmholtz coils generating a permanent magnetic field of 5mT (corresponding to 210 kHz). NMR signal is detected from a 3 ml water sample, doped with $CuSO_4$. We used a small concentration of paramagnetic ions, $CuSO_4$ to decrease the T_1 from 2 s to 200 ms, and the T_2 is also reduced by the same factor. The RF pulse is applied with a surface coil around the water sample, perpendicularly to the sensor. The mixed sensor used is a YBCO-based sensor with a gain larger than 700. It is located in a liquid nitrogen dewar, on top of the room temperature water sample. The distance between the sensor and the sample is 20 mm. The liquid nitrogen in the dewar can be pumped at 150 mbar to lower the sensor temperature to 67 K, in order to operate the sensor well below its transition temperature (around 80 K here). A room temperature low noise preamplifier is used for signal amplification, and acquisition is done via our homemade NMR spectrometer. The signal is scaled down using heterodyne detection.

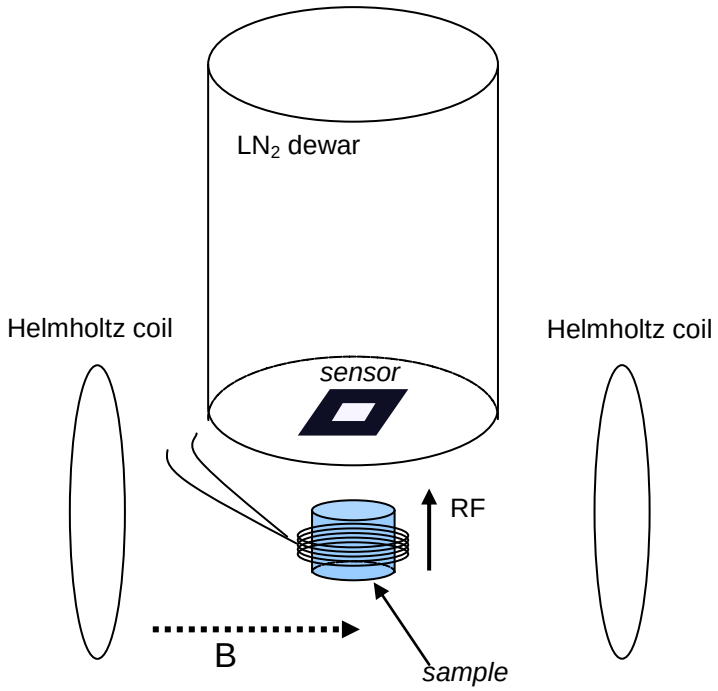

.

Figure 43: Schematics of the experimental setup. A main field (B) generated by Helmholtz coils is applied to the sample. An RF pulse is applied by a coil wound around the water sample at the corresponding frequency. The detection is done by a mixed sensor placed into a liquid nitrogen dewar.

The mixed sensor is placed in the 5 mT static field without any protection, nor any feedback loop. The static field applied in the plane of the sensor is far lower than the fields needed to demagnetize the hard layer (of order 1 T), but they can degrade the GMR sensitivity via its free layer. If the 5mT field is applied perpendicular to the yoke, the working point on the GMR characteristic ends at a point where the sensitivity is low (see Figure 4). When this 5 mT field is applied parallel to the yoke, the GMR characteristic has also a reduced slope. To compensate for the static field we can add a small (1*3 mm^2) NdFeB magnet on the GMR. This magnet generates a local field of 5 mT on the GMR elements, opposite to the applied B_0 field and does not affect the YBCO.

Sequences and NMR signals

A 100W RF pulse has been applied on the sensor during 50 µs, with a repetition time of 300 ms. During the pulse, saturation is reached in the sensor without destroying it. The sensor recovers in a microsecond range and is able to measure a signal right after the pulse. It can experience series of sequences without protection, thereby shortening the dead time of the system after the pulse. Figure 44 shows the same spin echo sequence detected either by a resonant coil or a mixed sensor. With the broadband mixed sensor we can detect the free induction decay (FID) signal from the nuclear spins, whereas with the tuned coil detector this signal is hidden by the coil ringing (spectrometer dead time).

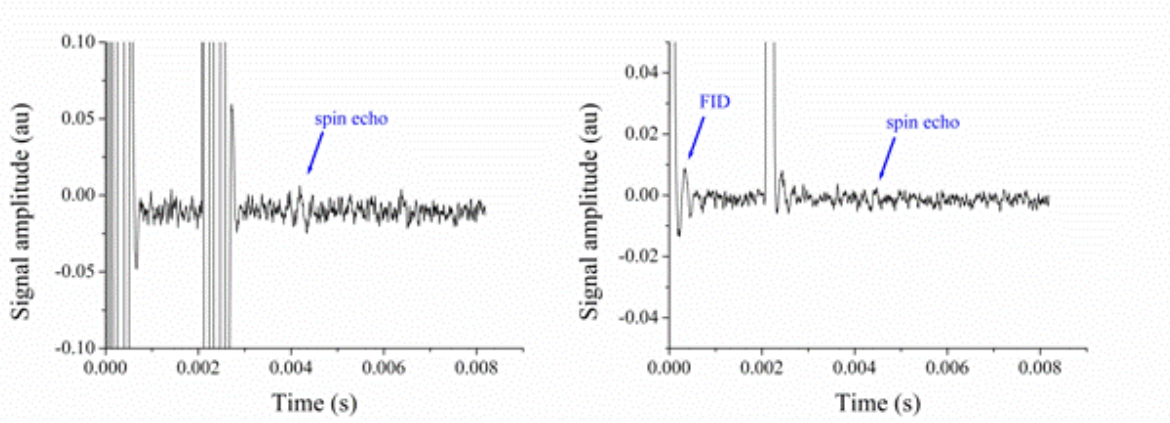

Figure 44: Comparison of the response of a resonant coil (left) and a mixed sensor (right) to a 100 W RF pulse of 50 µs at 210 kHz. The mixed sensor being untuned, one does not observe the same ringing as in the coil response. The recovery is very fast and the small oscillation (arrow) observed in the mixed sensor response is the nuclear free induction decay.

For further experiments, we have improved the sensitivity of the system by inserting a cooled flux transformer between the mixed sensor and the sample [34] . Figure 43 shows the comparison at 320 kHz between a signal obtained with a tuned coil and a unturned mixed sensor. We used a YBCO sensor with gain of 330 (built by Sensitec) and a flux transformer with a k coupling of 0.4.

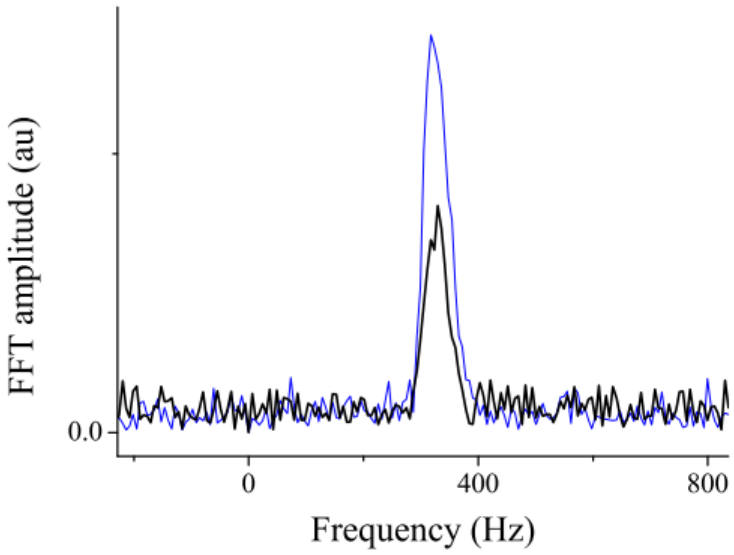

Figure 45: Signal of water detected with an untuned YBCO mixed sensor at 77 K (black) and a resonant coil (blue).

The NMR signal can be acquired few µs after switching the RF pulse off. This is a key point for detection of broad signals from solids [35] . Another possible use of the broadband nature of mixed sensor is the detection of multiple frequency signals from different nuclei or in multi-slicing MRI.

Experiments have been also realized with a pre-polarizing field of 1 T. The experimental setup consists of circulating doped water in a rubber pipe which passes through the aperture of a 1 T Halbach cylinder permanent magnet. The polarized water is then flowing in the NMR setup area, where the signal can be measured and averaged.

Discussion and perspectives on low-field MRI

NMR experiments have been successfully carried out, demonstrating the capability of mixed sensor to detect very low-field (5-8 mT) resonant signals of protons. With the present sensors and in this frequency range, the signal-to-noise ratio is more or less the same as the conventional resonant coil system. Therefore the mixed sensor sensitivity still has to be improved. First, the room temperature preamplifier is adding noise and, as for MEG and MCG, use of cold electronics for the first stage amplification would improve the detection. The sensor effective surface and distance to sample is also affecting the performances. The filling factor for NMR signal collection may be enhanced by the use of a flux transformer with a large pickup loop (see the NQR experiment). At 4 K, a Nb-based superconducting flux transformer can be easily implemented. At 77 K low noise flux transformers based on commercial High-T_C superconducting tapes are a possibility [34] but the coupling factor between the sensor and the input coil has to be studied in this configuration. Tuning the flux transformer [26] to the desired frequency could be an option to improve the sensitivity, but it has hard drawbacks on the broadband nature of the sensor.

The mixed sensor detectivity can also be improved and we aim to reduce it to 1 $fT/Hz^{1/2}$ or less. 2 fT/√Hz detectivity can be achieved with the same sensor cooled at 4 K followed by appropriate electronics. The sensor design can also be improved, by reducing the constriction size or using

different type of magnetoresistive sensor (e.g. a Magnetic Tunnel Junction). Ways to improve the sensor detectivity are developed in the perspectives.

An MRI setup has been recently built up to acquire 3D NMR images. The experimental setup comprises a homogeneous static field up to 10 mT (homogeneity 10 ppm) produced by a pair of Helmholtz coils. Three additional shimming coils compensate for the static external field inhomogeneities.

The technique to acquire an image is to apply field gradients during the pulses and the acquisition. As the frequency varies linearly as function of the field, a linear gradient induces a frequency directly proportional to the position of the detected volume. Hence time domain acquisition is the Fourier transform of the spatial image. The easiest image is simply a density image but by using specific sequences, it is possible to obtain images which are modified by T_1 or T_2 differences.

In our setup, three sets of small coils produce the field gradients necessary for the imaging. A picture of this setup is given in Figure 46. The volume which can be scanned is 5x5x5 cm^3.

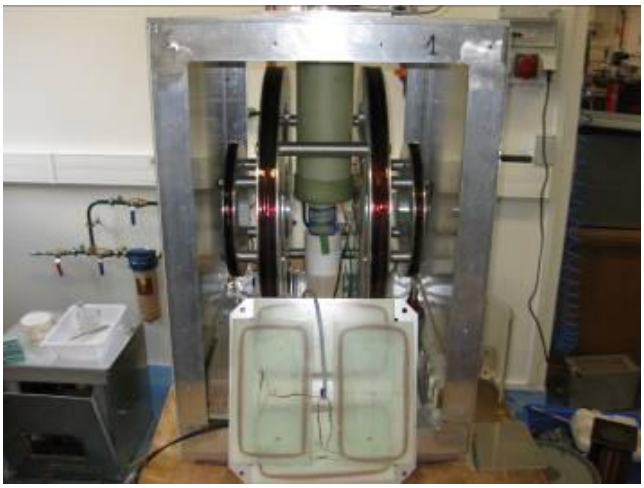

Figure 46: Picture of the MRI experimental setup built in our laboratory. The static field is generated by the largest copper coils. Smaller coils are the shimming coils. Gradients coils can be seen in front of the picture. A 5x5x5 cm^3 volume can be scanned in this setup.

We have added to the spectrometer the control of 3 gradients in order to perform full 3D MRI acquisitions. For obtaining 3D images, we can perform sequences similar to high field MRI sequences. The Figure 47 gives an example of such a sequence.

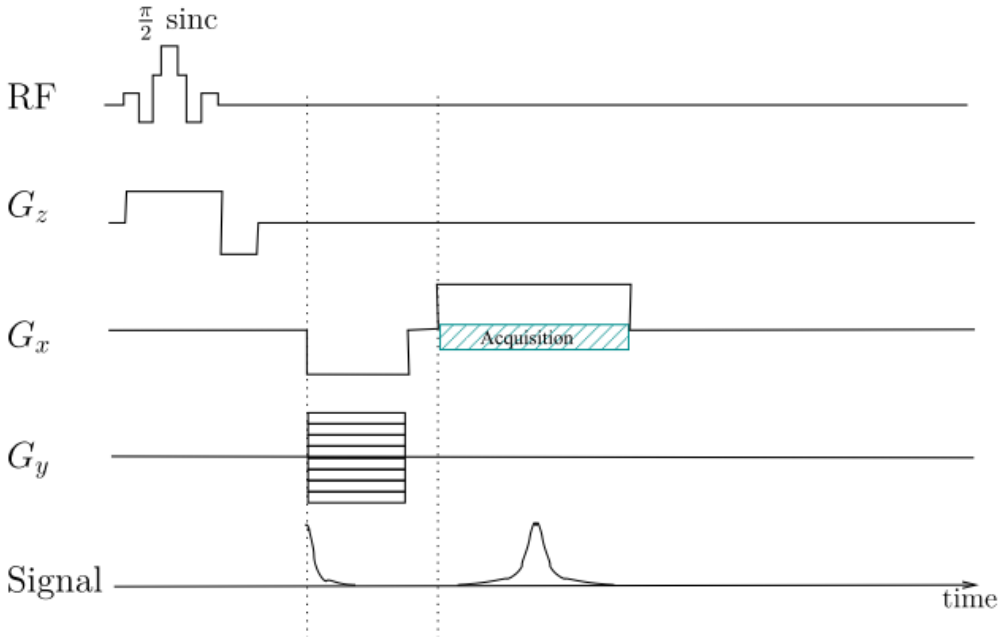

Figure 47: Sequence for obtaining a 3D image. The G_z gradient determines the slice. A soft pulse allows a good selection of the slice. G_x and G_y gradients are used to obtain a 2D image in the selected slice. G_y is used as a phase encoder and for example the image of Figure 48 is obtained with 64 values of G_y regularly spaced and the gradient G_x is used during the acquisition. G_x is used in an echo design.

First 3D images of fruits have been already obtained, as shown in Figure 48.

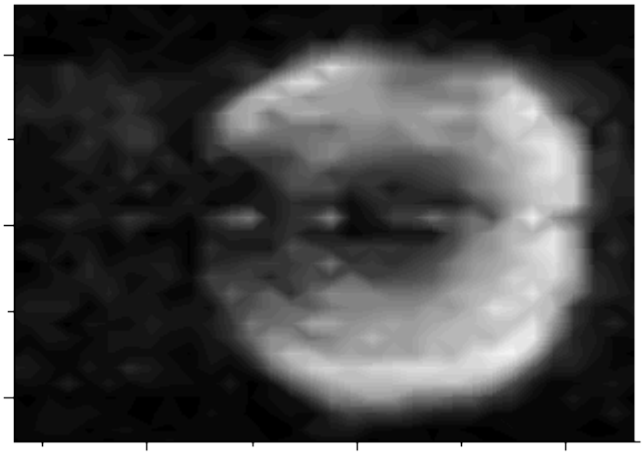

Figure 48 : 2D slice NMR image of a peach in an 8 mT (320 kHz) static field (homogeneity 10 ppm) with a tuned coil. Acquisition time is 10'. The dark part in the center is the stone; the black spot on the left side of the fruit was a damaged part.

We have very recently implemented mixed sensors on the MRI setup and first images with untuned mixed sensors on water have been obtained (Figure 49).

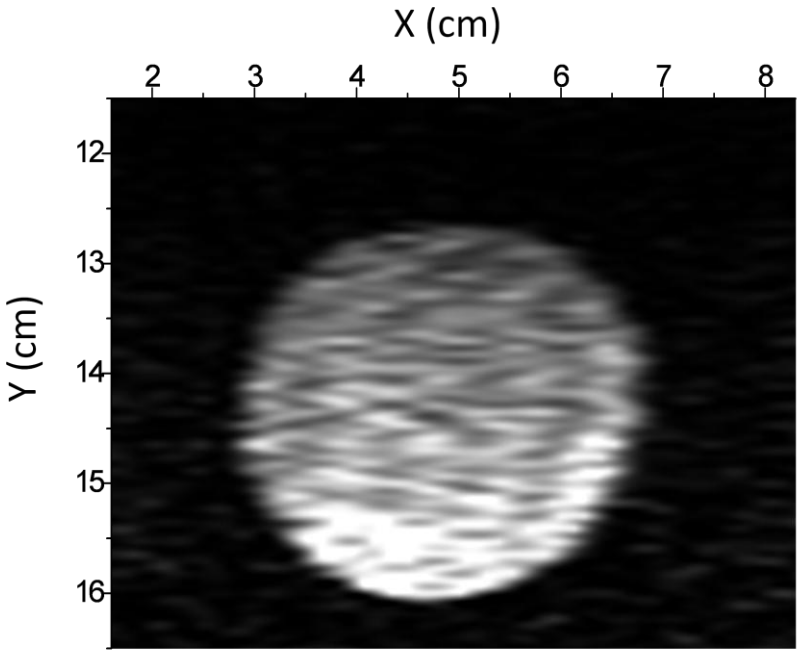

Figure 49 : Very first MRI obtained on a water tube with a YBCO sensor cooled at 77 K, for a 7 mT field (314 kHz).

Perspectives

Highly sensitive magnetometry requires sensors with a very good signal-to-noise ratio over a wide frequency range to fulfill various applications (biomagnetism, NMR…). Up to now three technologies fulfill this requirement: SQUIDs, which is the most mature, atomic magnetometry, recently proposed [36] and mixed sensors that I have developed since 2003.

Mixed sensors, combining a superconducting flux transformer to a sensitive GMR field sensing element reach detectivity level of the order of few fT/√Hz at 77 K in the thermal noise range typically from 1 kHz to several tens of MHz.

Improvements in terms of detectivity is a key issue to allow measurements in the low frequency range, in particular to realize MEG signal acquisition at 77 K, which would make this technology more competitive than present low-Tc SQUIDs. Ways to gain in sensitivity is presented in the first section.

Meanwhile, development of new setup combining anatomical and functional imaging is being carrying out, to offer new medical systems apparatus for brain studies. This ongoing work is presented in the second section.

Achieving subfemtotesla sensitivity

Improving the mixed sensor sensitivity and its detectivity level can be carried out by exploring the design and the materials aspect.

Design and fabrication

From calculations, we know that the sensitivity can be improved with a larger superconducting loop and a smaller constriction.

A larger loop is usually not desirable for applications where an array of sensors is required, like in MEG; otherwise the number of channels would be reduced. In applications where size does not matter, larger loop can be used. Therefore, larger surface sensor can be fabricated, but alternative solution can be advantageously chosen, in particular connecting the solid state flux transformer to an additional larger macroscopic loop. This can be applied in particular to Nb sensors (Figure 50), where a superconducting link can be efficiently performed between the Nb wire and the Nb thin film, as it is already developed for SQUIDs. This technique can also be used in a gradiometer configuration. MCG where few sensors are used and LF-MRI would benefit from this device.

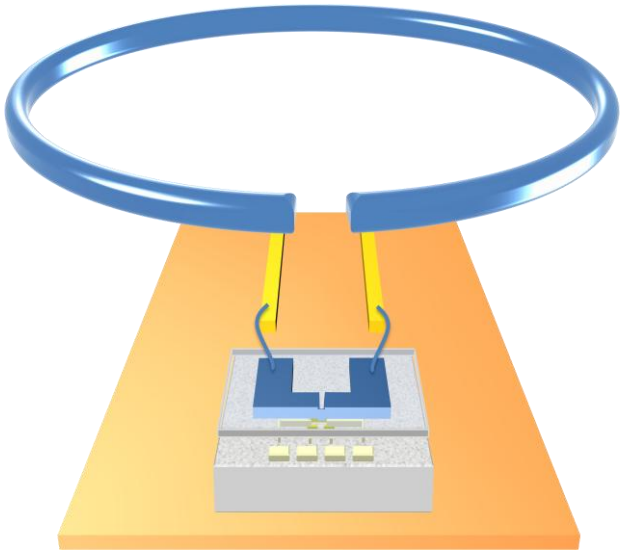

Figure 50: Schematics of a niobium mixed sensor where the total flux is enhanced by connecting superconductively the open superconducting loop of the sensor to a macroscopic pick up loop, made out of niobium wire.

Reducing the constriction would also lead to a detectivity enhancement. For a 25 mm large loop, reducing the constriction size from 5 to 1 µm would correspond to improving the gain by a factor of 5 –going from 3 fT/√Hz to 0.6 fT√Hz in the thermal noise (for a same GMR sensitivity). With conventional photolithography techniques, this can be achieved both on Nb and YBCO (devices with a 0.5 µm wide constriction have been achieved by Sensitec and operate successfully at 77 K). Reducing to submicron scale the constriction can be achieved with electronic lithography on Nb. Width of 100 or 200 nm should be feasible. YBCO being extremely sensitive to the oxygen contents, submicron etching is usually leading to degradation of the superconducting properties. An option to reduce the size of the constriction in a YBCO sensor would be to use ion irradiation technique. Oxygen and helium irradiation have been successfully applied to fabricate patterns down to 50 nm in YBCO [37] . Collaboration with Jérôme Lesueur at ESPCI has started to explore this way of improving the sensor performances.

An important point to keep in mind when reducing the size of the constriction is the fact that the GMR element is also reduced accordingly. Very small size MR elements are already used in read heads, but where linearity and low frequency noise are not an issue. In the case of our sensor, reducing the GMR width to 100 nm leads to reduce strongly the magnetic volume (50 times compared to a 5 µm element), which increases the low frequency noise by a factor 7 (Eq. 12). All these aspects should be carefully studied to determine the optimal width at which the sensor exhibits its best performances in a stable and low noise regime. One or two orders of magnitude in the detectivity should be a possible improvement by this way.

Materials

Improvement can be brought by the materials chosen for the sensor, and in particular for the MR element.

Tunnel Magneto Resistive (TMR) mixed sensors

First sensors have been fabricated with optimized GMR field sensing elements. GMR ratio is not larger than 10 to 20 % in the current-in-plane configuration (CIP), one can change the GMR element by a TMR element with an insulating MgO barrier, where MR up to 1000 % at room temperature have been demonstrated [38] . The patterning process is slightly different since the measurement configuration is current-perpendicular-to plane (CPP). In collaboration with Susana Cardoso (INSEC-MN, Lisbon), we have successfully realized and tested Nb-mixed sensors with MgO-TMR elements. These devices are properly responding to the applied field, but their sensitivity is limited by the low frequency noise of the TMR, whose 1/f knee is quite high (500 kHz) and by the output voltage in the TMR element, which was limited to about 0.2V (the magnetoresistance of the TMR element decreases when increasing the applied voltage, and the tunnel junction can be destroyed with voltages higher than 0.6 V). The output voltage of one junction is limited, and the TMR mixed sensor has therefore performances just as good as GMR mixed sensor. Nevertheless, the power consumption is much lower (100 times less), which make this alternative already very interesting for arrays of sensors where total consumption can be an issue (MEG application for instance).

One way to improve performances of TMR devices is to include several TMR elements in series, which is increasing the total magnetic volume, and therefore strongly reducing the 1/f ²noise. On room temperature TMR sensors, we have demonstrated sensitivity (without flux transformer) of 1 nT/√Hz at 1 Hz [39] .

AlOx-Magnetic Tunnel Junction (MTJ) could also be alternately implemented in mixed sensor. Even if their magnetoresistance is lower than MgO-MTJ (80 % at room temperature), they offer a deposition process with temperature that is compatible with YBCO, which is not the case of MgO-MTJ, which requires a 270°C annealing step to crystallize the MgO interface.

As spin electronics are developing very quickly these last years, we can benefit from the constant progress made in this area for our sensor development.

All oxide mixed sensors

In the area of magnetoresistive materials, some manganese-based oxides have exhibited remarkable properties with extremely high MR ratio (more than 500 % [40] [41]). Development of these materials for applications has been limited by the fact that they operate at rather low temperature (below 150K). In the particular case of mixed sensors, they would be well adapted. One candidate would be $La_{2/3}Sr_{1/3}MnO_3$ (LSMO), which could be integrated in a tunnel junction where the insulating barrier would be made out of $SrTiO_3$. In order to obtain different coercivities of the two electrodes, one of the LSMO layer can be doped with Ruthenium. We have recently measured the two different coercivities by means of SQUID magnetometry on such a trilayer [43] obtained by pulsed laser deposition at IEF by Philippe Lecoeur.

Noise measurements have to be performed with various designs of the junction to obtain the lowest noise figure possible.

One main advantage of this MTJ for mixed sensor is that the oxides used can be grown on a YBCO layer epitaxially, which will increase the chance to have very smooth interfaces, therefore good MR properties and low noise characteristics. Proposal of such an all-oxide sensor is shown in Figure 51.

For oxide junctions, the optimized stack should be patterned with the proper shape so there is a coherent rotation of the free layer without domain formation. The bottom and top contacts need also to be properly formed. Oxide-metallic contacts have to be optimized to insure no extra noise is brought in the system. Conventional lithography will be used in a first step. Reducing the size of the junction and of the YBCO constriction will be explored by means of ion irradiation in a second step.

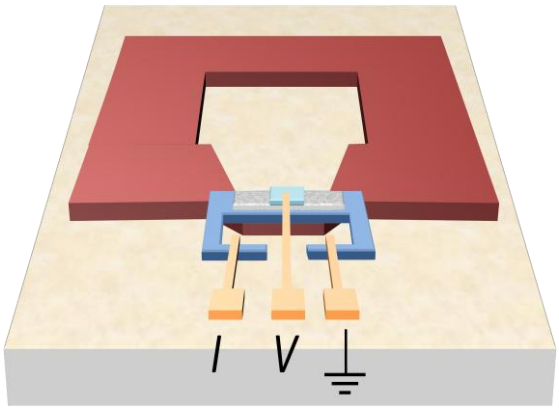

Figure 51 : Schematics of an all-oxide mixed sensor. The superconducting loop is patterned in a YBCO film grown on $SrTiO_3$ substrate. An insulating layer of STO (not shown on the figure) on the YBCO loop prevents short-cut of the MTJ with the loop. The MTJ is an LSMO/STO/LSMO(Ru) stack, connected in CPP configuration. The soft layer -LSMO- might be patterned in a shape which avoid magnetic domain.

Such all-oxide hybrid sensors would achieve sensitivities in the range of 100 attoteslas for a cm^2 surface which will be the most sensitive sensors ever achieved, and would operate at 77 K.

Realizing combined biomagnetic signal measurements and MRI

Development of new generations of sensors with better performances will be carried out in parallel with setting up whole measurement systems allowing very low field MRI together with biomagnetic signal acquisition. This new facility could be applied to cardiac monitoring system, where real-time information of polarization currents in the heart would be combined with anatomical information.

In a more complex system, sensor of arrays could be used to record the MEG signal, as in conventional MEG, together with LF-MRI which would give directly the anatomical information. So far both data are obtained by performing separately the information on an MEG system in a shielded room, then on a high field MRI. Precise localization of the MEG signal is possible only by reconstructing the brain position through reference points which should be the same in both experiments. This procedure is complicated and time consuming, and cannot be applied to patients with implanted electrodes like in Parkinson disease treatment. An MRI experiment could be run into the MEG experimental facility by the aim of mixed sensor cooled down on the same dewar as the MEG helmet. A first proposal of apparatus would be using low-Tc SQUIDs for the MEG recording, and a large Nb flux transformer connected with superconducting bonds to the half loop of a mixed sensor for the MRI signal acquisition. When the mixed sensor will reach sensitivity of few fT/√Hz at 1 Hz, possibly at 77 K, the whole apparatus could use mixed sensors for both MEG and LF-MRI.

The first step of this development is addressed by the European project MEGMRI [44] , involving twelve European teams. An artist's view of the future prototype is shown in Figure 52.

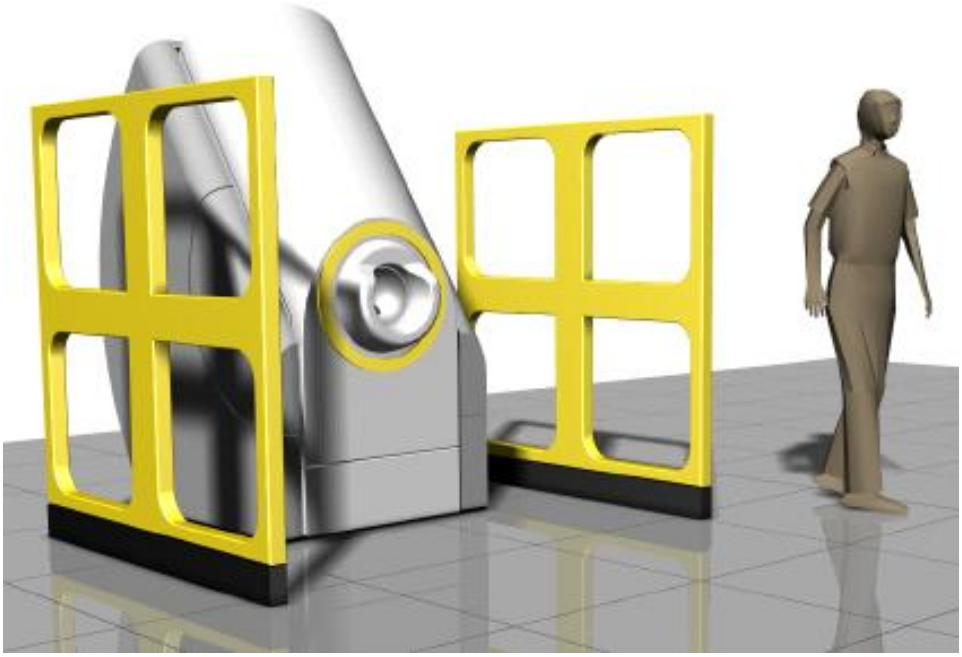

Figure 52 : Artistic view of a LF-MRI –MEG apparatus. The static field and gradient fields are generated by the large coils (in yellow on the sides). The MRI signal is measured by a large pickup coil inside the dewar where the sensors for MEG stands (small yellow coil around the MEG helmet).

Performing a whole head imaging combined with recording of a model MEG signal (evoked potential for instance) with mixed sensor will open perspective for a novel medical facility dedicated to knowledge of the brain and its functions.

References

[1] P. Ripka, *Magnetic sensors and magnetometers*, Artech House (2001)

[2] A.C. Rose-Innes and E.H. Rhoderick, „Introduction to Superconductivity", 2nd ed., 1978

[3] A.S. Edelstein *et al.* J. Appl. Phys. 99, 08B317 (2006)

[4] A. Guedes *et al*. IEEE Trans. On Magn. 44 (11) (2008)

[5] E.H. Brandt and G.P. Mikitik, Phys. Rev. Lett. **85**, 4164 (2000)

[6] M. Pannetier, et al. Sensors and Actuators A-PHYSICAL 129 (1-2): 146-149 (2006)

[7] R.J. Wijngaarden, K. Heeck, M. Welling, R. Limburg, M. Pannetier, K. van Zetten, V.L.G. Roorda and A.R. Voorwinden. Rev. of Sc. Instr. 72 (6) 2661-2664, (2001)

[8] S. Linzen *et al.* Physica C 372–376 (2002) 146–14

[9] F. Schmidt *et al*. Supercond. Sci. Technol. **15** (2002) 488–493

[10] M. Pannetier, C. Fermon, G. Le Goff, J. Simola, E. Kerr, Science, 304, 1648-1650 (2004)

[11] M. Pannetier, C. Fermon, G. Le Goff, J. Simola, E. Kerr and J.M.D. Coey. J.M.M.M. 290-292, 1158-1160 (2005)

[12] www.sensitec.com

[13] www.theva.com

[14] F.N. Hooge, Phys. Lett. 29A, 139 (1969)

[15] C. P. Bean,Rev. Mod. Phys. 36, 31 (1964)

[16] A.T. Fiory et al, Appl.Phys.Lett **52** 2165 (1988)

[17] J. Malmivuo & R. Plonsey: *Bioelectromagnetism - Principles and Applications of Bioelectric and Biomagnetic Fields*, Oxford University Press, New York, 1995.

[18] G. Baule, R. McFee, Am Heart J 1963; 66:95-96.

[19] D. Cohen, E.A. Edelsack, J.E. Zimmermann, Appl Phys Lett 1970;16:278-280. ; D. Cohen, Science 1967; 156:652-654.

[20] M. Hämäläinen et al, Rev. Mod. Phys. 65 (2) (1993)

[21] D. Cohen and E. Halgren, *Encyclopedia of Neuroscience* (2009), vol. 5, pp. 615-622

[22] P. Pollock, Canad. M. A.J. May 1, vol. 76 (1957)

[23] N. Biziere and C. Fermon, proceeding of JEMS 2006 conference

[24] J. Clarke, M. Hartridge and M. Mößle, Annu. Rev of Biomed. Eng. , vol. 9, pp. 389–413, 2007

[25] Y. S. Greenberg, Rev. Mod. Phys., vol. 70, no. 1, January 1998

[26] W. Myers, D. Slichter, M. Hatridge, S. Busch, M. Mößle, R. McDermott, A. Trabesinger, and J. Clarke, Journal of Magnetic Resonance, vol. 186, no. 2, pp. 182–192, June 2007.

[27] A.N. Garroway, M.L. Buess, J.P. Yesinowski, J.B. Miller and R.A. Krauss, Proc. SPIE, Vol. 2276, 139 (1994)

[28] M.L. Buess, A.N. Garroway, J.B. Miller : "detection of explosives by Nuclear Quadrupole Resonance", US Patent n°5206592 (April 1993)

[29] J.A.S Smith : "method and apparatus for detecting certain compounds", US Patent n°4887034 (December 1989)

[30] J. Barras, M.J. Gaskell, N. Hunt, R.I. Jenkinson, K.R. Mann, D.A.G. Pedder, G.N. Shilstoneand J.A.S. Smith, APPLIED MAGNETIC RESONANCE 25 (3-4): 411-437 2004

[31] VS Grechishkin, Appl. Phys. A55, 505-507 (1992).

[32] D.F. He, M. Tachiki, H. Itozaki, SUPERCONDUCTOR SCIENCE & TECHNOLOGY (2008).

[33] S.K. Lee, K.L. Sauer, S.J. Seltzer et al. APPLIED PHYSICS LETTERS, 89, (2006)

[34] H. Dyvorne, J. Scola, C. Fermon, J. F. Jacquinot, and M. Pannetier-Lecoeur, Rev. Sci. Instrum., vol. 79, pp. 025107-025111, Feb 2008.
[35] Melinda J. Duer, “Introduction to Solid-State NMR Spectroscopy”
[36] I. K. Kominis, T. W. Kornack, J. C. Allred, M. V. Romalis, Nature 422, 596 (2003)
[37] M. Sirena, S. Matzen, N. Bergeal, J. Lesueur, G. Faini, R. Bernard, J. Briatico and D. G. Crété, J. Appl. Phys. 105, 023910 (2009)
[38] L. Jiang et al., Appl. Phys. Express 2(8) 083002 (2009)
[39] R. Guerrero, M. Pannetier-Lecoeur, C. Fermon, S. Cardoso, R. Ferreira, and P. P. Freitas, J. Appl. Phys. 105(11) 113922 (2009)
[40] Viret M, Drouet M, Nassar J, et al. EUROPHYSICS LETTERS 39 (5): 545-549 SEP 1 1997
[41] X.W. Li, Yu Lu, G.Q. Gong, G. Xiao, A. Gupta, P. Lecoeur, J. Z. Sun, Y.Y. Wang, V.P. Dravid, J. of Appl. Phys. 81 (8), (1997)
[42] B. Raquet, J. M. D. Coey, S. Wirth and S. von Molnar, Phys Rev B 59 12435-12443 (1999)
[43] A. Solignac, Internship report, July 2009
[44] http://www.megmri.net/

Résumé

Afin de permettre la mesure de champs magnétiques extrêmement faibles, comme ceux produits par l'activité neuronale lors des taches cognitives, nous avons proposé et réalisé un capteur femtotesla (10^{-15}T) associant l'électronique de spin et la supraconductivité offrant une alternative en technologie couches minces et à 77K aux capteurs les plus sensibles actuellement que sont les SQUIDs (Superconducting Quantum Interference Devices) à basse température critique (4K).

Le principe de base de ces capteurs, appelés capteurs mixtes, repose sur l'association d'un transformateur flux-champ très performant, obtenu grâce à une large boucle supraconductrice comprenant une constriction, et d'un capteur magnétique de type GMR ou TMR métallique de grande sensibilité. Des niveaux de détectivité de quelques fT/√Hz dans le bruit thermique ont pu ainsi être atteints à l'azote liquide, ce qui est comparable aux performances des SQUIDs à l'hélium liquide. Il existe cependant un bruit en 1/f à basse fréquence, dû au faible volume de l'élément magnétorésistif, qui limite les performances du capteur en dessous de 1kHz. Des techniques de suppression de ce bruit basse fréquence par bascule sur des points de référence du capteur sont étudiées et permettent déjà de réduire ce bruit de plus d'un ordre de grandeur, ce qui permet d'atteindre 0.1pT/√Hz à 1Hz.

Grâce à ces capteurs, il a été possible de réaliser des premières mesures de la composante magnétique du signal cardiaque (signal de quelques pT/√Hz). Le très faible niveau de bruit thermique a permis également de réaliser des mesures de résonance quadrupolaire nucléaire sur des composés azotés qui est une technique de détection sélective d'explosifs. Nous avons aussi montré la possibilité de mesurer la résonance magnétique nucléaire du proton à très faible champ. Cela nous a conduit à développer un dispositif d'imagerie par résonance magnétique pour réaliser des images 3D à très bas champ (<20mT), ce qui présente un très grand intérêt pour la réalisation de systèmes d'IRM portables, faible coût, qu'il serait aussi possible d'intégrer dans un système de magnétoencéphalographie.

Abstract

In order to measure extremely weak magnetic fields, such as those produced by the neuronal activity during cognitive tasks in the brain, we have proposed and realized a femtotesla (10^{-15}T) sensor based on the association of spin electronics and superconductivity which offers an alternative in thin film technology and at 77K to the most sensitive devices which are low-T_C SQUIDs (Superconducting Quantum Interference Devices).

The principle of these mixed sensors is to combine an efficient flux-to-field transformer, realized by a large superconducting loop containing a constriction, and a magnetoresistive sensor with very good sensitivity (GMR or TMR). Field levels of few fT/√Hz in the thermal noise have been reached at liquid nitrogen temperature, which is comparable to performances of SQUIDs in liquid helium. Performances are nevertheless reduced in the low frequency (below 1kHz) range due to 1/f noise present because of the small volume of the magnetoresistive element. Cancellation techniques based on switching on and off the sensor to reference points have been developed and already allow reducing the low frequency noise of more than one order of magnitude, leading to sensitivity in field of 0.1pT/√Hz at 1Hz.

First measurements of the magnetic component of the cardiac signal (few pT/√Hz at 1Hz) have been acquired with mixed sensors. The very low thermal noise level has also allowed realizing nuclear quadrupolar resonance measurements on nitrogen compounds, which is a non invasive detection technique for solid explosives. We have also achieved first proton Low-Field Nuclear Magnetic Resonance experiments with such sensors, which has led to develop and build a Magnetic Resonance Imaging setup to realize 3D images at low field (<20mT), which is of great interest for low cost and portable equipment development.